Research Article

Rashid Ali, Rabia Imtiaz, Moin-ud-Din Junjua*, Fuad A. Awwad, Emad A. A. Ismail, and Ahmed S. Hendy

Fractal formation and chaotic soliton phenomena in nonlinear conformable Heisenberg ferromagnetic spin chain equation

https://doi.org/10.1515/phys-2025-0166
received March 24, 2025; accepted May 13, 2025

Abstract: The present study constructs and investigates solitonic phenomena in the complex structured (3+1)-dimensional conformable Heisenberg ferromagnetic spin chain equation (CHFSCE). This model explains the behavior of ferromagnetic spin chains and is an extension of the integer-order Heisenberg equation in nonlinear physics that controls the magnetization of the ferromagnetic solid. We present a new array of soliton solutions in the form exponential, rational, hyperbolic, and rational-hyperbolic functions, using the Riccati modified extended simple equation method (RMESEM). The proposed anstaz uses a complex structured wave transformation to convert CHFSCE into a more manageable nonlinear ordinary differential equation (NODE) and constraint conditions. The resulting NODE is assumed to have a close form solution that further converts it into a system of nonlinear algebraic equations *via* substitution in order to identify fresh plethora of optical soliton solutions. Moreover, the fundamental characteristics and theory of the employed conformable derivative, specifically, the chain rule, have been described. We demonstrate the existence of quasi-periodic solitons, including smooth-, multiple-, and periodic-periodic solitons, in the context of CHFSCE using a range of 3D, 2D, and contour visual representations. The obtained quasi-periodic solitons prominently result in the development of fractal structures while their squared norms result in the development of hump, peakon, and parabolic solitons. Additionally, we investigate bifurcating and chaotic behavior, detecting its existence in the perturbed dynamical system and finding advantageous results that suggest quasi-periodicity and fractal behavior in the model. According to the results we obtained, the suggested strategy is a powerful method for detecting novel soliton phenomena in such types of nonlinear settings.

Keywords: nonlinear fractional partial differential equations, conformable fractional derivatives, Riccati modified extended simple equation method, quasi-periodic solitons

1 Introduction

The study begins by framing the intended model inside the context of its earlier findings and providing a thorough analysis of pertinent literature. In this section, the main goals of the study are outlined, knowledge gaps highlighted, and the study's organizational structure is explained.

1.1 Overview and background of the conformable Heisenberg ferromagnetic spin chain equation (CHFSCE)

Nonlinear fractional partial differential equations (NFPDEs) have become increasingly important for modeling and presenting complex phenomena as they allow for the precise capture of the memory and inherited characteristics of the system being modelled. These mathematical equations are particularly helpful in explaining anomalous diffusion phenomena and have wide-ranging applications in disciplines such as biology, physics, chemistry, finance, engineering,

* **Corresponding author: Moin-ud-Din Junjua,** School of Mathematical Sciences, Zhejiang Normal University, Jinhua 321004, Zhejiang, P.R. China, e-mail: moinuddin@zjnu.edu.cn
Rashid Ali: School of Information and Mathematics, Yangtze University, Jingzhou, Hubei, 434023, China
Rabia Imtiaz: Department of Mathematics, University of Engineering and Technology, Lahore 39161, Pakistan
Fuad A. Awwad, Emad A. A. Ismail: Department of Quantitative Analysis, College of Business Administration, King Saud University, P.O. Box 71115, Riyadh 11587, Saudi Arabia
Ahmed S. Hendy: Department of Computational Mathematics and Computer Science, Institute of Natural Sciences and Mathematics, Ural Federal University, 19 Mira St., Yekaterinburg 620002, Russia; Department of Mechanics and Mathematics, Western Caspian University, Baku 1001, Azerbaijan

and economics [1–6]. The problem of comprehending and evaluating the dynamics of NFPDEs, which describe a broad range of complex phenomena in numerous scientific domains, has captured the attention of scientists and researchers in the fields of mathematics and physics as a result of their applications. However, the nonlinearity and nonlocality of fractional derivatives pose unique challenges for their interpretation and resolution. The solution and analysis of these equations may require the development of unique approaches and tools, as typical analytical and numerical processes can occasionally not be pertinent. In spite of these challenges, research on NFPDEs has led to major breakthroughs in various areas of scientific and engineering domains [7–9]. The emergence of novel analytical and numerical methods [10–14] for solving and evaluating NFPDEs has expanded research prospects and enhanced our comprehension of complex systems [15–17].

The study of soliton solutions is an intriguing development in NFPDE's research in recent years. Soliton solutions are remarkable solitary wave solutions to NFPDEs, which possess unique and stable properties [18–21]. These solutions differ significantly from regular waves and offer crucial insights into the behavior of nonlinear systems. Comprehending and characterizing solitons have been the main topics of current research attention. Researchers have worked hard to identify novel solitons in a variety of nonlinear systems in addition to understanding the fundamental characteristics of solitons. Analytical techniques such as the Sardar sub-equation technique [22], tan-function method [23], the Kudryashov methodology [24], the Khater approach [25], the sub-equation strategy [26], the extended direct algebraic method (EDAM) [27,28], $(\frac{G'}{G})$-expansion approach [29], exp-function approach [30], amongst others [31–37], have been significant in these discoveries by providing the mathematical tools needed to explore these complex wave phenomena. While these approaches greatly advance our knowledge of soliton dynamics and assist us in connecting them to the theories that explain phenomena, it is crucial to acknowledge that they may have drawbacks and restrictions (*e.g.*, the seven common mistakes) [38,39]. Moreover, several of these methods depend on the Riccati equation [40]. Since the Riccati equation has solitary solutions, these techniques are useful for studying soliton phenomena in nonlinear models [41].

Recent developments in soliton theory, especially fractal soliton theory [42–44], which examines the complex relationship between solitons and fractals, have led to intriguing new avenues for mathematical research. A fractal soliton is a stable, constrained wave packet that possesses both a solitonic and a fractal structure. Fractal solitons are nonuniform bordered solitons that display complex geometric patterns at different sizes and self-replicate at a steady pace. Insights into nonlinear processes in physics, engineering, and biology can be gained by connecting soliton with fractal geometry [45–47]. As a result, the concept of fractal soliton has several real-world uses across a range of fields. Because of their unique property, fractal solitons are helpful in the study of chaos theory as they help us comprehend the dynamics and resilience of chaotic systems. Fractal soliton research is becoming more popular in modern mathematics, and as it develops, new concepts in theoretical and practical mathematics should be supported.

The present work investigates and analyzes new plethora of soliton solutions for (3+1)-dimensional CHFSCE, which is a prominent complex structured NFPDE with intricate interactions between fractional derivatives and magnetic spins. This nonlinear Schrödinger-type equation was developed by Latha and Vasanthi [48] to explain nonlinear waves inside the Heisenberg ferromagnetic spin chain system by combining the logical state ansatz with the Holstein–Primakoff bosonic analysis of spin operators. This model is represented as follows [35,49]:

$$\begin{aligned} &\iota \mathfrak{D}_t^{\delta} s + \rho_1 \mathfrak{D}_x^{\alpha}(\mathfrak{D}_x^{\alpha} s) + \rho_2 \mathfrak{D}_y^{\beta}(\mathfrak{D}_y^{\beta} s) + \rho_3 \mathfrak{D}_x^{\alpha}(\mathfrak{D}_y^{\beta} s) \\ &\quad - \rho_4 |s|^2 s = 0, \end{aligned} \tag{1}$$

where $\mathfrak{D}_t^{\delta}(\circ)$, $\mathfrak{D}_x^{\alpha}(\circ)$, and $\mathfrak{D}_y^{\beta}(\circ)$ are conformable fractional derivatives (CFDs), $\rho_1 = (\kappa + \kappa_2)\nu^4$, $\rho_2 = (\kappa_1 + \kappa_2)\nu^4$, $\rho_3 = 2\kappa_2\nu^4$, $\rho_4 = 2B\nu^4$, $s \equiv s(x, y, t)$, $0 < \delta, \alpha, \beta \leq 1$, ν is the lattice structure parameter, κ_2 represents the adjacent interaction along the diagonal length, B is the anisotropy parameter of the uniaxial crystal field while κ and κ_1, respectively, are the corresponding coefficients of the bilinear exchange interactions in the x and y-axes.

1.2 Literature review of the CHFSCE

Many other academics have used various numerical and analytical techniques to handle (1) in both fractional and integer senses prior to this scholarly study. For example, the (G'/G)-expansion approach was utilized by Ullah *et al.* [35] to obtain kink, periodic, multiple periodic, and shock soliton solutions for (1). Ma *et al.* [49] created a number of exact solutions, including doubly periodic, periodic, bright, and dark soliton solutions in the form of hyperbolic function, Jacobi elliptic function exponential and trigonometric function for (1) in integer form, by using the Jacobi elliptic method and the improved F-expansion method. In another research effort, Devnath *et al.* [50] used $(G'/G, 1/G)$-expansion and extended Kudryashov methods to generate some general and novel solutions in the form of trigonometric functions, bell-shaped functions, and their rational forms, revealing the existence of singular periodic, periodic, kink,

flat kink, and V-shaped solitons in the context of CHFSCE with β-order derivative. Finally, Hashemi used the simplest equation and Nucci's approach to report bright and dark solitons with other precise solutions for time-fractional conformable CHFSCE [51].

Researchers have recently concentrated greatly on analyzing the chaotic and bifurcating features of nonlinear models using concepts from knot theory [52,53]. In order to show that the model underlying the perturbed dynamical system exhibits bifurcating and chaotic behavior, a number of techniques from the corpus of previous research are employed. Lyapunov exponent method [54], Lyapunov spectrum theory [55], time series method [56], Poinćare map method [57], and phase portrait method [58] are a few of these approaches. When bifurcation and chaotic theories are used for the study of nonlinear systems, the dynamics and stability of models and their solutions are better understood. Moreover, they are used to examine how a change in a parameter affects the qualitative behavior of a system and its solutions. A great deal of research has been done in this field. Using the Galilean transformation, for instance, Muflih Alqahtani *et al.* produced a number of conventional results, including sensitivity, bifurcations analysis, and chaotic flows [59]. Similarly, Hosseini *et al.* [60] performed a more comprehensive study of a generalized Schrödinger equation by using the theory of the planar dynamical system to carry out its bifurcation and the Galilean transformation to derive the dynamical system of the governing equation. By considering a perturbed component in the resulting dynamical system, several two- and three-dimensional phase portraits are provided, further examining the existence of chaotic behaviors of the model. In another study, Iqbal *et al.* developed a Hamiltonian dynamical system from the leading equations for the nonlinear electrical transmission lines in order to analyze the bifurcation characteristics with chaos and nonlinear coherent structures for the voltage wave propagation [55]. Additionally, they used the Lyapunov spectrum theory to support the existence of chaos in the targeted model. Inspired by the current study of nonlinear model analysis, the Galilean transformation technique and time series approach are used to examine the chaotic behavior of the perturbed dynamical systems of CHFSCE, noting its existence in the dynamical system that has been perturbed and obtaining favorable outcomes about the chaotic behaviors of CHFSCE.

1.3 Research gap in the present investigation

As the literature cited above demonstrates, soliton dynamics in CHFSCE have been examined earlier, but no investigation has been conducted to look into and assess how fractals are formed when solitons undergo periodic oscillations inside the intended model. This finding points to a sizable gap in the corpus of existing knowledge. Our work closes this gap by offering a thorough and unique analysis of the fractal solitonic phenomena in the model using the suggested Riccati modified extended simple equation method (RMESEM).

1.4 Objectives and aims of the research

The study's goals and objectives are as follows: The intended CHFSCE will first be transformed *via* a complex transformation into a single manageable nonlinear ordinary differential equation (NODE). Next, we will convert the NODE into an algebraic system of equations by supposing a series-form solution and using the RMESEM. Finally, the system will be examined using the Maple tool to determine the CHFSCE's soliton solutions. The necessary conditions for the existence of these solutions will also be described in detail. Our results demonstrate the existence of smooth-, multiple-, and periodic-periodic solitons in the context of CHFSCE, which lead to the formation of fractal structures. On the other hand, the squared norms of the acquired periodic solitons result in the emergence of hump, peakon, and parabolic solitons. These findings are presented using a range of 3D, 2D, and contour visual representations. We also study bifurcating and chaotic behavior, observing its presence in the perturbed dynamical system and obtaining favorable outcomes that imply fractal and quasi-periodic motion. Our results show that, in the context of such nonlinear situations, the suggested technique is a powerful tool for detecting novel soliton phenomena.

1.5 Layout of the current research

The remaining study is arranged as follows: The resources and the working mechanism of the suggested RMESEM are covered in Section 2. Section 3 presents the CHFSCE's soliton solutions. A discussion and numerous graphs are given in Section 4. Our findings are summarized in Section 5, and an appendix is given after that.

2 Materials and methods

The definition of CFD and the operational mechanism of the RMESEM are given in this section.

2.1 Description of CFD

By using CFD's advantage over alternative fractional derivative operators, we can find soliton solutions for NFPDEs. For example, since they do not obey the chain rule [61,62], different fractional derivative forms are unable to yield the soliton solutions of CHFSCE stated in (1). As a result, fractional derivatives in (1) were defined in the sense of CFDs. The expression for this derivative operator with order α is as follows [63]:

$$\mathfrak{D}_{\mathfrak{Z}}^{\alpha} f(\mathfrak{Z}) = \lim_{\alpha \to 0} \frac{f(\alpha \mathfrak{Z}^{1-\alpha} + \mathfrak{Z}) - f(\mathfrak{Z})}{\alpha}, \quad \alpha \in (0, 1]. \tag{2}$$

In this investigation, the properties of this derivative given below are employed:

$$\mathfrak{D}_{\mathfrak{Z}}^{\alpha} \mathfrak{Z}^{m} = m \mathfrak{Z}^{m-\alpha}, \tag{3}$$

$$\mathfrak{D}_{\mathfrak{Z}}^{\alpha}(m_1 \varrho(\mathfrak{Z}) \pm m_2 \eta(\mathfrak{Z})) = m_1 \mathfrak{D}_{\mathfrak{Z}}^{\alpha}(\varrho(\mathfrak{Z})) \pm m_2 \mathfrak{D}_{\mathfrak{Z}}^{\alpha}(\eta(\mathfrak{Z})), \tag{4}$$

$$\mathfrak{D}_{\mathfrak{Z}}^{\alpha} \varrho[\eta(\mathfrak{Z})] = \varrho'_{\eta}(\eta(\mathfrak{Z})) \mathfrak{D}_{\mathfrak{Z}}^{\alpha} \eta(\mathfrak{Z}), \tag{5}$$

where $\varrho(\mathfrak{Z})$ and $\eta(\mathfrak{Z})$ are arbitrary differentiable functions, whereas m, m_1 and m_2 denote constants.

Proposition 2.1. *Let $f(\mathfrak{Z})$ and $g(\mathfrak{Z})$ be two differentiable functions, then*

$$\mathfrak{D}_{\mathfrak{Z}}^{\beta} f[g(\mathfrak{Z})] = f'_{g}(g(\mathfrak{Z})) \mathfrak{D}_{\mathfrak{Z}}^{\beta} g(\mathfrak{Z}).$$

Proof. In a neighborhood $\mathfrak{Z}_0$, if the function g is constant, then $\mathfrak{D}_{\mathfrak{Z}}^{\beta} f(g(\mathfrak{Z}_0)) = 0$. On the other hand, we assume the following for the nonconstant function g near $\mathfrak{Z}_0$. Here for every $\mathfrak{Z}_1, \mathfrak{Z}_2 \in (\mathfrak{Z}_0 - \gamma_0, \mathfrak{Z}_0 + \gamma_0)$, we can discover a $\gamma > 0 \ni g(\mathfrak{Z}_1) \neq g(\mathfrak{Z}_2)$. Since g is continuous at $\mathfrak{Z}_0$, we may obtain, for $\mathfrak{Z}_0 > a$, $\mathfrak{Z}_0^{\beta} \neq a$ (where $a \geq 0$).

$$\begin{aligned}
\mathfrak{D}_{\mathfrak{Z}}^{\beta}(f \circ g)(\mathfrak{Z}_0) &= \lim_{\gamma \to 0} \frac{f(g(\mathfrak{Z}_0 + \gamma \mathfrak{Z}_0^{-\beta}(\mathfrak{Z}_0 - a))) - f(g(\mathfrak{Z}_0))}{\gamma(1 - a\mathfrak{Z}_0^{-\beta})} \\
&= \lim_{\gamma \to 0} \frac{f(g(\mathfrak{Z}_0 + \gamma \mathfrak{Z}_0^{-\beta}(\mathfrak{Z}_0 - a))) - f(g(\mathfrak{Z}_0))}{g(\mathfrak{Z}_0 + \gamma \mathfrak{Z}_0^{-\beta}(\mathfrak{Z}_0 - a)) - g(\mathfrak{Z}_0)} \\
&\quad \cdot \frac{g(\mathfrak{Z}_0 + \gamma \mathfrak{Z}_0^{-\beta}(\mathfrak{Z}_0 - a)) - g(\mathfrak{Z}_0)}{\gamma(1 - a\mathfrak{Z}_0^{-\beta})} \\
&= \lim_{\gamma_1 \to 0} \frac{f(g(\mathfrak{Z}_0) + \gamma_1) - f(g(\mathfrak{Z}_0))}{\gamma_1} \\
&\quad \cdot \frac{g(\mathfrak{Z}_0 + \gamma \mathfrak{Z}_0^{-\beta}(\mathfrak{Z}_0 - a)) - g(\mathfrak{Z}_0)}{\gamma(1 - a\mathfrak{Z}_0^{-\beta})} \\
&= f'(g(\mathfrak{Z}_0)) \mathfrak{D}_{\mathfrak{Z}}^{\beta}(g)(\mathfrak{Z}_0).
\end{aligned}$$

The chain rule is thus satisfied by CFD. □

2.2 Working methodology of RMESEM

The Riccati equation is the foundation of many analytical techniques. These techniques may be used for the investigation of solitary wave phenomena in nonlinear models as the Riccati equation contains solitary solutions [41]. The current work, which incorporates the Riccati equation with RMESEM to generate and assess solitary wave dynamics in the CHFSCE, was inspired by these applications of the Riccati hypothesis. In this section, we outline the RMESEM's mechanism [34]. Look at the following NPDE:

$$\begin{aligned}
&A(\mathfrak{S}, \mathfrak{D}_t^{\delta} \mathfrak{S}, \mathfrak{D}_{\tau_1}^{\alpha} \mathfrak{S}, \mathfrak{D}_{\tau_2}^{\beta} \mathfrak{S}, \mathfrak{S}\mathfrak{D}_{\tau_1}^{\alpha} \mathfrak{S}, \ldots) = 0, \\
&\alpha, \beta, \delta \in (0, 1],
\end{aligned} \tag{6}$$

where $\mathfrak{S} = \mathfrak{S}(t, \tau_1, \tau_2, \tau_3, \ldots, \tau_r)$.

The steps listed below will be taken to address (6):

1. The first step involves performing a variable-form transformation $\mathfrak{S}(t, \tau_1, \tau_2, \tau_3, \ldots, \tau_r) = \mathfrak{H}(\mathfrak{Z})$, where $\mathfrak{Z}$ has several representations. The following NODE is obtained by transforming equation (6) in this way:

$$B(\mathfrak{H}, \mathfrak{H}'\mathfrak{H}, \mathfrak{H}', \ldots) = 0, \tag{7}$$

where $\mathfrak{H}' = \frac{d\mathfrak{H}}{d\mathfrak{Z}}$. Sometimes, the NODE is integrated one or several times to satisfy the homogeneous balance condition (7).

2. Next utilizing the solution of the extended Riccati-NODE, the resulting closed form solution for the NODE in (7) is proposed

$$\mathfrak{H}(\mathfrak{Z}) = \sum_{j=0}^{\gamma} b_j \left(\frac{U'(\mathfrak{Z})}{U(\mathfrak{Z})}\right)^j + \sum_{j=0}^{\gamma-1} a_j \left(\frac{U'(\mathfrak{Z})}{U(\mathfrak{Z})}\right)^j \cdot \left(\frac{1}{U(\mathfrak{Z})}\right). \tag{8}$$

In this solution, $b_j (j = 0, \ldots, \gamma)$ and $a_j (j = 0, \ldots, \gamma - 1)$ indicates the constants that are needed to be found, and $U(\mathfrak{Z})$ indicates the solution to the resultant extended Riccati-NODE

$$U'(\mathfrak{Z}) = p + qU(\mathfrak{Z}) + r(U(\mathfrak{Z}))^2, \tag{9}$$

where p, q, and r are constants.

3. We obtain the positive integer γ needed in Eq. (8) by homogeneously balancing the greatest nonlinear component and the highest-order derivative in Eq. (7).

4. Following that, all the terms of $U(\mathfrak{Z})$ are combined into an equal ordering after substituting (8) in (7), or in the equation that emerges from the integration of (7) which generates an expression in $U(\mathfrak{Z})$. An algebraic system of equations in $b_j (j = 0, \ldots, \gamma)$ and $a_j (j = 0, \ldots, \gamma - 1)$ with additional accompanying parameters is obtained when the coefficients in the resulting expression are set to zero.

5. With Maple, the set of nonlinear algebraic equations is solved analytically.

6. To acquire analytical soliton solutions for (6), the next step is to calculate and enter the undetermined values with $U(\mathfrak{Z})$ (the Eq. (9) solution) in Eq. (8). We might potentially use the general solution of (9) to derive other sets of soliton solutions. These clusters are shown in Table 1.

3 Execution of RMESEM

In this section, we apply our proposed approach to CHFSCE in (1) in order to obtain soliton solutions for it. We start with the complex transformation that follows:

$$s(x,y,t) = e^{\iota\psi}S(\mathfrak{Z}), \quad \mathfrak{Z} = \frac{\sigma_1 x^{\alpha}}{\alpha} + \frac{\sigma_2 y^{\beta}}{\beta} - \frac{ct^{\delta}}{\delta}, \quad \psi = \frac{\varrho_1 x^{\alpha}}{\alpha} + \frac{\varrho_2 y^{\beta}}{\beta} - \frac{\omega t^{\delta}}{\delta}, \tag{10}$$

where σ_i, $\varrho_i (j = 1, 2)$, ω, and c are constants. Substituting (10) in (1) and splitting the real and imaginary components yield the following equations:

$$(\omega - \rho_1 l_1^2 - \rho_3\varrho_2\varrho_1 - \rho_2 l_2^2)S + (\rho_1 k_1^2 - \rho_3\sigma_2\sigma_1 - \rho_2 k_2^2)S'' - \rho_4 S^3 = 0 \tag{11}$$

and

$$(2\rho_1\varrho_1\sigma_1 + 2\rho_2\varrho_2\sigma_2 + \varrho_2\sigma_1 + \rho_3(\varrho_1\sigma_2) - c)S' = 0. \tag{12}$$

Eq. (12) yields the following constraint condition:

$$c = (2\rho_1\varrho_1\sigma_1 + 2\rho_2\varrho_2\sigma_2 + \varrho_2\sigma_1 + \rho_3(\varrho_1\sigma_2)). \tag{13}$$

Applying this constraint, the system in (11) and (12) is hence reduced to the single NODE displayed below:

Table 1: Particular solutions $U(\mathfrak{Z})$ of Riccati equation in (9) and the formation of $\frac{U'(\mathfrak{Z})}{U(\mathfrak{Z})}$

S. No.	Cluster	Constraint(s)	$U(\mathfrak{Z})$	$\left(\frac{U'(\mathfrak{Z})}{U(\mathfrak{Z})}\right)$
1	Trigonometric solutions	$\mathfrak{G} < 0, r \neq 0$	$-\frac{q}{2r} + \frac{\sqrt{-\mathfrak{G}}\tan\left(\frac{1}{2}\sqrt{-\mathfrak{G}}\,\mathfrak{Z}\right)}{2r}$,	$-\frac{1}{2}\frac{\mathfrak{G}\left(1+\left(\tan\left(\frac{1}{2}\sqrt{-\mathfrak{G}}\,\mathfrak{Z}\right)\right)^2\right)}{-q+\sqrt{-\mathfrak{G}}\tan\left(\frac{1}{2}\sqrt{-\mathfrak{G}}\,\mathfrak{Z}\right)}$,
			$-\frac{q}{2r} - \frac{\sqrt{-\mathfrak{G}}\cot\left(\frac{1}{2}\sqrt{-\mathfrak{G}}\,\mathfrak{Z}\right)}{2r}$,	$\frac{1}{2}\frac{\left(1+\left(\cot\left(\frac{1}{2}\sqrt{-\mathfrak{G}}\,\mathfrak{Z}\right)\right)^2\right)\mathfrak{G}}{q+\sqrt{-\mathfrak{G}}\cot\left(\frac{1}{2}\sqrt{-\mathfrak{G}}\,\mathfrak{Z}\right)}$,
			$-\frac{q}{2r} + \frac{\sqrt{-\mathfrak{G}}(\tan(\sqrt{-\mathfrak{G}}\,\mathfrak{Z}) + (\sec(\sqrt{-\mathfrak{G}}\,\mathfrak{Z})))}{2r}$,	$\frac{-\mathfrak{G}(1+\sin(\sqrt{-\mathfrak{G}}\,\mathfrak{Z}))\sec(\sqrt{-\mathfrak{G}}\,\mathfrak{Z})}{-q\cos(\sqrt{-\mathfrak{G}}\,\mathfrak{Z})+\sqrt{-\mathfrak{G}}\sin(\sqrt{-\mathfrak{G}}\,\mathfrak{Z})+\sqrt{-\mathfrak{G}}}$,
			$-\frac{q}{2r} + \frac{\sqrt{-\mathfrak{G}}(\tan(\sqrt{-\mathfrak{G}}\,\mathfrak{Z}) - (\sec(\sqrt{-\mathfrak{G}}\,\mathfrak{Z})))}{2r}$.	$\frac{\mathfrak{G}(\sin(\sqrt{-\mathfrak{G}}\,\mathfrak{Z})-1)\sec(\sqrt{-\mathfrak{G}}\,\mathfrak{Z})}{-q\cos(\sqrt{-\mathfrak{G}}\,\mathfrak{Z})+\sqrt{-\mathfrak{G}}\sin(\sqrt{-\mathfrak{G}}\,\mathfrak{Z})-\sqrt{-\mathfrak{G}}}$.
2	Hyperbolic solutions	$\mathfrak{G} > 0, \quad r \neq 0$	$-\frac{q}{2r} - \frac{\sqrt{\mathfrak{G}}\tanh\left(\frac{1}{2}\sqrt{\mathfrak{G}}\,\mathfrak{Z}\right)}{2r}$,	$-\frac{1}{2}\frac{\left(-1+\left(\tanh\left(\frac{1}{2}\sqrt{\mathfrak{G}}\,\mathfrak{Z}\right)\right)^2\right)\mathfrak{G}}{q+\sqrt{\mathfrak{G}}\tanh\left(\frac{1}{2}\sqrt{\mathfrak{G}}\,\mathfrak{Z}\right)}$,
			$-\frac{q}{2r} - \frac{\sqrt{\mathfrak{G}}(\tanh(\sqrt{\mathfrak{G}}\,\mathfrak{Z}) + i(\mathrm{sech}(\sqrt{\mathfrak{G}}\,\mathfrak{Z})))}{2r}$,	$-\frac{\mathfrak{G}(-1+i\sinh(\sqrt{\mathfrak{G}}\,\mathfrak{Z}))}{\cosh(\sqrt{\mathfrak{G}}\,\mathfrak{Z})(q\cosh(\sqrt{\mathfrak{G}}\,\mathfrak{Z})+\sqrt{\mathfrak{G}}\sinh(\sqrt{\mathfrak{G}}\,\mathfrak{Z})+i\sqrt{\mathfrak{G}})}$,
			$-\frac{q}{2r} - \frac{\sqrt{\mathfrak{G}}(\tanh(\sqrt{\mathfrak{G}}\,\mathfrak{Z}) - i(\mathrm{sech}(\sqrt{\mathfrak{G}}\,\mathfrak{Z})))}{2r}$,	$-\frac{\mathfrak{G}(1+i\sinh(\sqrt{\mathfrak{G}}\,\mathfrak{Z}))}{\cosh(\sqrt{\mathfrak{G}}\,\mathfrak{Z})(-q\cosh(\sqrt{\mathfrak{G}}\,\mathfrak{Z})-\sqrt{\mathfrak{G}}\sinh(\sqrt{\mathfrak{G}}\,\mathfrak{Z})+i\sqrt{\mathfrak{G}})}$,
			$-\frac{q}{2r} - \frac{\sqrt{\mathfrak{G}}(\coth(\sqrt{\mathfrak{G}}\,\mathfrak{Z}) + (\mathrm{csch}(\sqrt{\mathfrak{G}}\,\mathfrak{Z})))}{2r}$.	$-\frac{1}{4}\frac{\mathfrak{G}\left(2\left(\cosh\left(\frac{1}{4}\sqrt{\mathfrak{G}}\,\mathfrak{Z}\right)\right)^2-1\right)}{\theta(-2q\theta+\sqrt{\mathfrak{G}})}$.
3	Rational solutions	$\mathfrak{G} = 0$	$-2\frac{p(q\mathfrak{Z}+2)}{q^2\mathfrak{Z}}$,	$-2\frac{1}{\mathfrak{Z}(q\mathfrak{Z}+2)}$,
		$\mathfrak{G} = 0, \& q = r = 0$	$\mathfrak{Z}p$,	$\frac{1}{\mathfrak{Z}}$,
		$\mathfrak{G} = 0, \& q = p = 0$	$-\frac{1}{\mathfrak{Z}r}$.	$-\frac{1}{\mathfrak{Z}}$.
4	Exponential solutions	$r = 0, \& q = m, p = lm$	$e^{m\mathfrak{Z}} - l$,	$\frac{me^{m\mathfrak{Z}}}{e^{m\mathfrak{Z}}-b}$,
		$p = 0, \& q = m, r = lm$	$\frac{e^{m\mathfrak{Z}}}{1-le^{m\mathfrak{Z}}}$.	$-\frac{m}{-1+le^{m\mathfrak{Z}}}$.
5	Rational-hyperbolic solutions	$r \neq 0, \& q \neq 0, p = 0$	$-\frac{qk_1}{r(\cosh(q\mathfrak{Z})-\sinh(q\mathfrak{Z})+k_2)}$,	$\frac{q(\sinh(q\mathfrak{Z})-\cosh(q\mathfrak{Z}))}{-\cosh(q\mathfrak{Z})+\sinh(q\mathfrak{Z})-k_2}$,
			$-\frac{q(\cosh(q\mathfrak{Z})+\sinh(q\mathfrak{Z}))}{r(\cosh(q\mathfrak{Z})+\sinh(q\mathfrak{Z})+k_2)}$.	$\frac{qk_2}{\cosh(q\mathfrak{Z})+\sinh(q\mathfrak{Z})+k_2}$.

Moreover, $k_1, k_2 \in \mathrm{R}$, $\mathfrak{G} = q^2 - 4rp$, and $\theta = \cosh\left(\frac{1}{4}\sqrt{\mathfrak{G}}\,\mathfrak{Z}\right)\sinh\left(\frac{1}{4}\sqrt{\mathfrak{G}}\,\mathfrak{Z}\right)$.

$$S'' - \left(\frac{\rho_1 \varrho_1^2 + \rho_2 \varrho_2^2 + \rho_3 \varrho_1 \varrho_2 - \omega}{\rho_1 \sigma_1^2 + \rho_2 \sigma_2^2 + \rho_3 \sigma_1 \sigma_2}\right) S - \left(\frac{\rho_4}{\rho_1 \sigma_1^2 + \rho_2 \sigma_2^2 + \rho_3 \sigma_1 \sigma_2}\right) S^3 = 0. \tag{14}$$

We may determine $\gamma = 1$ by evaluating the homogeneous balance between S'' and S^3. When this value of γ is entered in Eq. (8), the RMESEM produces the ensuing series-form solution for Eq. (14):

$$S(\zeta) = \sum_{j=0}^{1} b_j \left(\frac{U'(\zeta)}{U(\zeta)}\right)^j + \frac{a_0}{U(\zeta)}. \tag{15}$$

We may infer an expression in terms of $U(\zeta)$ by substituting (15) for (14) and collecting all terms that have the same powers of $U(\zeta)$. If we set all the coefficients to zero, we obtain a system of nonlinear algebraic equations. The following sets of solutions are found by using Maple to solve the aforementioned system of nonlinear equations:

Case 1

$$\begin{aligned}
&b_0 = \frac{1}{2}\frac{q a_0}{p}, b_1 = 0, a_0 = a_0, \varrho_1 = \varrho_1,\\
&\varrho_2 = \varrho_2, \sigma_1 = \sigma_1, \sigma_2 = \sigma_2,\\
&\omega = \frac{-\nu^4}{2p^2\sigma_1^2}(-2\varrho_1^2 B a_0^2 + 2\varrho_1^2 p^2 \sigma_2^2 \kappa_1 + 2\varrho_1^2 \kappa_2 p^2 \sigma_2^2 - B q^2 a_0^2 \sigma_1^2 - 2\varrho_2^2 \kappa_1 p^2 \sigma_1^2 - 2\varrho_2^2 p^2 \sigma_1^2 \kappa_2\\
&\quad + 4\varrho_1^2 \kappa_2 p^2 \sigma_1 \sigma_2 + 4pr\sigma_1^2 B a_0^2 - 4\kappa_2 \varrho_1 \varrho_2 p^2 \sigma_1^2),\\
&\kappa = \frac{-2p^2\kappa_2\sigma_1\sigma_2 - p^2\sigma_1^2\kappa_2 - p^2\sigma_2^2\kappa_1 - p^2\sigma_2^2\kappa_2 + B a_0^2}{p^2\sigma_1^2}, \kappa_1 = \kappa_1, \kappa_2 = \kappa_2.
\end{aligned} \tag{16}$$

Case 2

$$\begin{aligned}
&b_0 = -\frac{1}{2}\Omega q, \quad b_1 = \Omega, \quad a_0 = -\Omega p,\\
&\varrho_1 = \varrho_1, \varrho_2 = \varrho_2, \sigma_1 = \sigma_1, \sigma_2 = \sigma_2,\\
&\omega = \frac{-\nu^4}{2}(-q^2\sigma_1^2\kappa_2 - q^2\sigma_2^2\kappa_2 - q^2\sigma_2^2\kappa_1 - q^2\sigma_1^2\kappa - 2q^2\kappa_2\sigma_1\sigma_2 + 4pr\sigma_2^2\kappa_1 + 4pr\sigma_2^2\kappa_2 - 4\kappa_2\varrho_1\varrho_2 + 8pr\kappa_2\sigma_1\sigma_2 - 2\kappa\varrho_1^2\\
&\quad - 2\varrho_1^2\kappa_2 - 2\varrho_2^2\kappa_1 - 2\kappa_2\varrho_2^2 + 4pr\sigma_1^2\kappa + 4pr\sigma_1^2\kappa_2).
\end{aligned} \tag{17}$$

Case 3

$$\begin{aligned}
&b_0 = \frac{-b_1 q}{2}, b_1 = b_1, a_0 = -b_1 p, \varrho_1 = \varrho_1,\\
&\varrho_2 = \varrho_2, \sigma_1 = 0, \sigma_2 = \sigma_2,\\
&\kappa = \kappa, \kappa_1 = \frac{B b_1^2 - \sigma_2^2\kappa_2}{\sigma_2^2}, \kappa_2 = \kappa_2,\\
&\omega = -\frac{1}{2}\frac{\nu^4(-B b_1^2 q^2\sigma_2^2 + 4pr\sigma_2^2 B b_1^2 - 4\kappa_2\varrho_1\varrho_2\sigma_2^2 - 2\kappa\varrho_1^2\sigma_2^2 - 2\varrho_1^2\kappa_2\sigma_2^2 - 2\varrho_2^2 B b_1^2)}{\sigma_2^2}.
\end{aligned} \tag{18}$$

Case 4

$$\begin{aligned}
&b_0 = \frac{1}{2}\Omega q, b_1 = 0, a_0 = \Omega p, \varrho_1 = \varrho_1,\\
&\varrho_2 = \varrho_2, \sigma_1 = \sigma_1, \sigma_2 = \sigma_2,\\
&\omega = \frac{-\nu^4}{2}(-q^2\sigma_1^2\kappa_2 - q^2\sigma_2^2\kappa_2 - q^2\sigma_2^2\kappa_1 - q^2\sigma_1^2\kappa - 2q^2\kappa_2\sigma_1\sigma_2 + 4pr\sigma_2^2\kappa_1 + 4pr\sigma_2^2\kappa_2 - 4\kappa_2\varrho_1\varrho_2 + 8pr\kappa_2\sigma_1\sigma_2 - 2\kappa\varrho_1^2\\
&\quad - 2\varrho_1^2\kappa_2 - 2\varrho_2^2\kappa_1 - 2\kappa_2\varrho_2^2 + 4pr\sigma_1^2\kappa + 4pr\sigma_1^2\kappa_2).
\end{aligned} \tag{19}$$

Case 5

$$\begin{aligned}
&b_0 = b_0, b_1 = b_1, a_0 = a_0, \varrho_1 = \varrho_1,\\
&\varrho_2 = \varrho_2, \sigma_1 = \sigma_1, \sigma_2 = 0, \nu = \nu,\\
&\omega = -2\kappa\nu^4\varrho_1\varrho_2 + \nu^4\varrho_2^2\kappa_1 - \nu^4\varrho_2^2\kappa,\\
&\kappa_1 = \kappa_1, \kappa_2 = -\kappa, B = 0,
\end{aligned} \tag{20}$$

where $\Omega = \sqrt{\frac{\sigma_1^2\kappa + 2\kappa_2\sigma_1\sigma_2 + \sigma_2^2\kappa_1 + \sigma_2^2\kappa_2 + \sigma_1^2\kappa_2}{B}}$.

Assuming case 1, we gain the resulting soliton solution clusters for (1).

Cluster 1.1: When $\mathfrak{G} < 0$ $r \neq 0$,

$$s_{1,1}(x,y,t) = e^{i\psi}\left(\frac{1}{2}\frac{qa_0}{p} + a_0\left(-\frac{1}{2}\frac{q}{r} + \frac{1}{2}\frac{\sqrt{-\mathfrak{G}}\tan\left(\frac{1}{2}\sqrt{-\mathfrak{G}}\,\mathfrak{Z}\right)}{r}\right)^{-1}\right), \tag{21}$$

$$s_{1,2}(x,y,t) = e^{i\psi}\left(\frac{1}{2}\frac{qa_0}{p} + a_0\left(-\frac{1}{2}\frac{q}{r} - \frac{1}{2}\frac{\sqrt{-\mathfrak{G}}\cot\left(\frac{1}{2}\sqrt{-\mathfrak{G}}\,\mathfrak{Z}\right)}{r}\right)^{-1}\right), \tag{22}$$

$$s_{1,3}(x,y,t) = e^{i\psi}\left(\frac{1}{2}\frac{qa_0}{p} + a_0\left(-\frac{1}{2}\frac{q}{r} + \frac{1}{2}\frac{\sqrt{-\mathfrak{G}}(\tan(\sqrt{-\mathfrak{G}}\,\mathfrak{Z}) + \sec(\sqrt{-\mathfrak{G}}\,\mathfrak{Z}))}{r}\right)^{-1}\right), \tag{23}$$

and

$$s_{1,4}(x,y,t) = e^{i\psi}\left(\frac{1}{2}\frac{qa_0}{p} + a_0\left(-\frac{1}{2}\frac{q}{r} + \frac{1}{2}\frac{\sqrt{-\mathfrak{G}}(\tan(\sqrt{-\mathfrak{G}}\,\mathfrak{Z}) - \sec(\sqrt{-\mathfrak{G}}\,\mathfrak{Z}))}{r}\right)^{-1}\right). \tag{24}$$

Cluster 1.2: When $\mathfrak{G} > 0$ $r \neq 0$,

$$s_{1,5}(x,y,t) = e^{i\psi}\left(\frac{1}{2}\frac{qa_0}{p} + a_0\left(-\frac{1}{2}\frac{q}{r} - \frac{1}{2}\frac{\sqrt{\mathfrak{G}}\tanh\left(\frac{1}{2}\sqrt{\mathfrak{G}}\,\mathfrak{Z}\right)}{r}\right)^{-1}\right), \tag{25}$$

$$s_{1,6}(x,y,t) = e^{i\psi}\left(\frac{1}{2}\frac{qa_0}{p} + a_0\left(-\frac{1}{2}\frac{q}{r} - \frac{1}{2}\frac{\sqrt{\mathfrak{G}}(\tanh(\sqrt{\mathfrak{G}}\,\mathfrak{Z}) + i\operatorname{sech}(\sqrt{\mathfrak{G}}\,\mathfrak{Z}))}{r}\right)^{-1}\right), \tag{26}$$

$$s_{1,7}(x,y,t) = e^{i\psi}\left(\frac{1}{2}\frac{qa_0}{p} + a_0\left(-\frac{1}{2}\frac{q}{r} - \frac{1}{2}\frac{\sqrt{\mathfrak{G}}(\tanh(\sqrt{\mathfrak{G}}\,\mathfrak{Z}) - i\operatorname{sech}(\sqrt{\mathfrak{G}}\,\mathfrak{Z}))}{r}\right)^{-1}\right), \tag{27}$$

and

$$s_{1,8}(x,y,t) = e^{i\psi}\left(\frac{1}{2}\frac{qa_0}{p} + a_0\left(-\frac{1}{2}\frac{q}{r} - \frac{1}{4}\frac{\sqrt{\mathfrak{G}}\left(\tanh\left(\frac{1}{4}\sqrt{\mathfrak{G}}\,\mathfrak{Z}\right) - \coth\left(\frac{1}{4}\sqrt{\mathfrak{G}}\,\mathfrak{Z}\right)\right)}{r}\right)^{-1}\right). \tag{28}$$

Cluster 1.3: When $\mathfrak{G} = 0$, $q \neq 0$,

$$s_{1,9}(x,y,t) = e^{i\psi}\left(\frac{1}{2}\frac{qa_0}{p} - \frac{1}{2}\frac{a_0q^2\mathfrak{Z}}{p(q\mathfrak{Z}+2)}\right). \tag{29}$$

Cluster 1.4: When $\mathfrak{G} = 0$, in case when $q = r = 0$,

$$s_{1,10}(x,y,t) = e^{i\psi}\left(\frac{a_0}{p\mathfrak{Z}}\right). \tag{30}$$

Cluster 1.5: When $q = m$, $p = lm(l \neq 0)$, and $r = 0$,

$$s_{1,11}(x,y,t) = e^{i\psi}\left(\frac{1}{2}\frac{a_0}{l} + \frac{a_0}{e^{m\mathfrak{Z}} - l}\right). \tag{31}$$

In the above solutions, $\mathfrak{Z} = \frac{\sigma_1 x^\alpha}{\alpha} + \frac{\sigma_2 y^\beta}{\beta} - \frac{(2\rho_1\varrho_1\sigma_1 + 2\rho_2\varrho_2\sigma_2 + \varrho_2\sigma_1 + \rho_3(\varrho_1\sigma_2))t^\delta}{\delta}$, $\psi = \frac{\varrho_1 x^\alpha}{\alpha} + \frac{\varrho_2 y^\beta}{\beta} - \frac{\omega t^\delta}{\delta}$, where ω is defined in (16).

Assuming case 2, we gain the resulting soliton solution clusters for (1).

Cluster 2.1: When $\mathfrak{G} < 0$, $r \neq 0$,

$$s_{2,1}(x,y,t)=e^{i\psi}\left(-\frac{1}{2}\Omega q-\frac{1}{2}\frac{\Omega\mathfrak{G}\left(1+\left(\tan\left(\frac{1}{2}\sqrt{-\mathfrak{G}}\,\mathfrak{Z}\right)\right)^2\right)}{-q+\sqrt{-\mathfrak{G}}\tan\left(\frac{1}{2}\sqrt{-\mathfrak{G}}\,\mathfrak{Z}\right)}-\frac{\Omega p}{\left(-\frac{1}{2}\frac{q}{r}+\frac{1}{2}\frac{\sqrt{-\mathfrak{G}}\tan\left(\frac{1}{2}\sqrt{-\mathfrak{G}}\,\mathfrak{Z}\right)}{r}\right)}\right),\tag{32}$$

$$s_{2,2}(x,y,t)=e^{i\psi}\left(-\frac{1}{2}\Omega q+\frac{1}{2}\frac{\Omega\mathfrak{G}\left(1+\left(\cot\left(\frac{1}{2}\sqrt{-\mathfrak{G}}\,\mathfrak{Z}\right)\right)^2\right)}{q+\sqrt{-\mathfrak{G}}\cot\left(\frac{1}{2}\sqrt{-\mathfrak{G}}\,\mathfrak{Z}\right)}-\frac{\Omega p}{\left(-\frac{1}{2}\frac{q}{r}-\frac{1}{2}\frac{\sqrt{-\mathfrak{G}}\cot\left(\frac{1}{2}\sqrt{-\mathfrak{G}}\,\mathfrak{Z}\right)}{r}\right)}\right),\tag{33}$$

$$\begin{aligned}s_{2,3}(x,y,t)=e^{i\psi}\Bigg(&\frac{-\Omega\mathfrak{G}(1+\sin(\sqrt{-\mathfrak{G}}\,\mathfrak{Z}))}{\cos(\sqrt{-\mathfrak{G}}\,\mathfrak{Z})(-q\cos(\sqrt{-\mathfrak{G}}\,\mathfrak{Z})+\sqrt{-\mathfrak{G}}\sin(\sqrt{-\mathfrak{G}}\,\mathfrak{Z})+\sqrt{-\mathfrak{G}})}\\&-\Omega p\left(-\frac{1}{2}\frac{q}{r}+\frac{1}{2}\frac{\sqrt{-\mathfrak{G}}(\tan(\sqrt{-\mathfrak{G}}\,\mathfrak{Z})+\sec(\sqrt{-\mathfrak{G}}\,\mathfrak{Z}))}{r}\right)^{-1}-\frac{1}{2}\Omega q\Bigg),\end{aligned}\tag{34}$$

and

$$\begin{aligned}s_{2,4}(x,y,t)=e^{i\psi}\Bigg(&\frac{\Omega\mathfrak{G}(\sin(\sqrt{-\mathfrak{G}}\,\mathfrak{Z})-1)}{\cos(\sqrt{-\mathfrak{G}}\,\mathfrak{Z})(-q\cos(\sqrt{-\mathfrak{G}}\,\mathfrak{Z})+\sqrt{-\mathfrak{G}}\sin(\sqrt{-\mathfrak{G}}\,\mathfrak{Z})-\sqrt{-\mathfrak{G}})}\\&-\Omega p\left(-\frac{1}{2}\frac{q}{r}+\frac{1}{2}\frac{\sqrt{-\mathfrak{G}}(\tan(\sqrt{-\mathfrak{G}}\,\mathfrak{Z})-\sec(\sqrt{-\mathfrak{G}}\,\mathfrak{Z}))}{r}\right)^{-1}-\frac{1}{2}\Omega q\Bigg).\end{aligned}\tag{35}$$

Cluster 2.2: When $\mathfrak{G}>0$ $r\neq 0$,

$$s_{2,5}(x,y,t)=e^{i\psi}\left(-\frac{1}{2}\Omega q-\frac{1}{2}\frac{\Omega\mathfrak{G}\left(-1+\left(\tanh\left(\frac{1}{2}\sqrt{\mathfrak{G}}\,\mathfrak{Z}\right)\right)^2\right)}{q+\sqrt{\mathfrak{G}}\tanh\left(\frac{1}{2}\sqrt{\mathfrak{G}}\,\mathfrak{Z}\right)}-\frac{\Omega p}{\left(-\frac{1}{2}\frac{q}{r}-\frac{1}{2}\frac{\sqrt{\mathfrak{G}}\tanh\left(\frac{1}{2}\sqrt{\mathfrak{G}}\,\mathfrak{Z}\right)}{r}\right)}\right),\tag{36}$$

$$\begin{aligned}s_{2,6}(x,y,t)=e^{i\psi}\Bigg(&\frac{-\Omega\mathfrak{G}(-1+i\sinh(\sqrt{\mathfrak{G}}\,\mathfrak{Z}))}{\cosh(\sqrt{\mathfrak{G}}\,\mathfrak{Z})(q\cosh(\sqrt{\mathfrak{G}}\,\mathfrak{Z})+\sqrt{\mathfrak{G}}\sinh(\sqrt{\mathfrak{G}}\,\mathfrak{Z})+i\sqrt{\mathfrak{G}})}\\&-\Omega p\left(-\frac{1}{2}\frac{q}{r}-\frac{1}{2}\frac{\sqrt{\mathfrak{G}}(\tanh(\sqrt{\mathfrak{G}}\,\mathfrak{Z})+i\operatorname{sech}(\sqrt{\mathfrak{G}}\,\mathfrak{Z}))}{r}\right)^{-1}-\frac{1}{2}\Omega q\Bigg),\end{aligned}\tag{37}$$

$$\begin{aligned}s_{2,7}(x,y,t)=e^{i\psi}\Bigg(&\frac{-\Omega\mathfrak{G}(1+i\sinh(\sqrt{\mathfrak{G}}\,\mathfrak{Z}))}{\cosh(\sqrt{\mathfrak{G}}\,\mathfrak{Z})(-q\cosh(\sqrt{\mathfrak{G}}\,\mathfrak{Z})-\sqrt{\mathfrak{G}}\sinh(\sqrt{\mathfrak{G}}\,\mathfrak{Z})+i\sqrt{\mathfrak{G}})}\\&-\Omega p\left(-\frac{1}{2}\frac{q}{r}-\frac{1}{2}\frac{\sqrt{\mathfrak{G}}(\tanh(\sqrt{\mathfrak{G}}\,\mathfrak{Z})-i\operatorname{sech}(\sqrt{\mathfrak{G}}\,\mathfrak{Z}))}{r}\right)^{-1}-\frac{1}{2}\Omega q\Bigg),\end{aligned}\tag{38}$$

and

$$s_{2,8}(x,y,t)=e^{i\psi}\left(\frac{-\Omega\mathfrak{G}\left(2\left(\cosh\left(\frac{1}{4}\sqrt{\mathfrak{G}}\,\mathfrak{Z}\right)\right)^2-1\right)}{4\cosh\left(\frac{1}{4}\sqrt{\mathfrak{G}}\,\mathfrak{Z}\right)\sinh\left(\frac{1}{4}\sqrt{\mathfrak{G}}\,\mathfrak{Z}\right)\left(-2q\cosh\left(\frac{1}{4}\sqrt{\mathfrak{G}}\,\mathfrak{Z}\right)\sinh\left(\frac{1}{4}\sqrt{\mathfrak{G}}\,\mathfrak{Z}\right)+\sqrt{\mathfrak{G}}\right)}\right.$$
$$\left.-\Omega p\left(-\frac{1}{2}\frac{q}{r}-\frac{1}{4}\frac{\sqrt{\mathfrak{G}}\left(\tanh\left(\frac{1}{4}\sqrt{\mathfrak{G}}\,\mathfrak{Z}\right)-\coth\left(\frac{1}{4}\sqrt{\mathfrak{G}}\,\mathfrak{Z}\right)\right)}{r}\right)^{-1}-\frac{1}{2}\Omega q\right). \tag{39}$$

Cluster 2.3: When $\mathfrak{G}=0$, $q\neq 0$,

$$s_{2,9}(x,y,t)=e^{i\psi}\left(-\frac{1}{2}\Omega q-2\frac{\Omega}{\mathfrak{Z}(q\mathfrak{Z}+2)}+\frac{1}{2}\frac{\Omega q^2\mathfrak{Z}}{q\mathfrak{Z}+2}\right). \tag{40}$$

Cluster 2.4: When $\mathfrak{G}=0$, in case when $q=p=0$,

$$s_{2,10}(x,y,t)=-e^{i\psi}\left(\frac{\Omega}{\mathfrak{Z}}\right). \tag{41}$$

Cluster 2.5: When $q=m$, $p=lm(l\neq 0)$, and $r=0$,

$$s_{2,11}(x,y,t)=e^{i\psi}\left(-\frac{1}{2}\Omega m+\frac{\Omega m e^{m\mathfrak{Z}}}{e^{m\mathfrak{Z}}-l}-\frac{\Omega m l}{e^{m\mathfrak{Z}}-l}\right). \tag{42}$$

Cluster 2.6: When $q=m$, $r=lm(l\neq 0)$, and $p=0$,

$$s_{2,12}(x,y,t)=-e^{i\psi}\left(\frac{\Omega m}{-1+le^{m\mathfrak{Z}}}\right). \tag{43}$$

Cluster 2.7: When $p=0$, $r\neq 0$, and $q\neq 0$,

$$s_{2,13}(x,y,t)=e^{i\psi}\left(-\frac{1}{2}\Omega q+\frac{\Omega q(\sinh(q\mathfrak{Z})-\cosh(q\mathfrak{Z}))}{-\cosh(q\mathfrak{Z})+\sinh(q\mathfrak{Z})-k_2}\right), \tag{44}$$

and

$$s_{2,14}(x,y,t)=e^{i\psi}\left(-\frac{1}{2}\Omega q+\frac{\Omega q k_2}{\cosh(q\mathfrak{Z})+\sinh(q\mathfrak{Z})+k_2}\right). \tag{45}$$

In the above solutions, $\mathfrak{Z}=\frac{\sigma_1 x^\alpha}{\alpha}+\frac{\sigma_2 y^\beta}{\beta}-\frac{(2\rho_1\varrho_1\sigma_1+2\rho_2\varrho_2\sigma_2+\varrho_2\sigma_1+\rho_3(\varrho_1\sigma_2))t^\delta}{\delta}$, $\psi=\frac{\varrho_1 x^\alpha}{\alpha}+\frac{\varrho_2 y^\beta}{\beta}-\frac{\omega t^\delta}{\delta}$, where ω is defined in (17).

Assuming case 3, we gain the resulting soliton solution clusters for (1):

Cluster 3.1: When $\mathfrak{G}<0$, $r\neq 0$,

$$s_{3,1}(x,y,t)=e^{i\psi}\left(-\frac{1}{2}b_1q-\frac{1}{2}\frac{b_1\mathfrak{G}\left(1+\left(\tan\left(\frac{1}{2}\sqrt{-\mathfrak{G}}\,\mathfrak{Z}\right)\right)^2\right)}{-q+\sqrt{-\mathfrak{G}}\tan\left(\frac{1}{2}\sqrt{-\mathfrak{G}}\,\mathfrak{Z}\right)}-\frac{b_1p}{\left(-\frac{1}{2}\frac{q}{r}+\frac{1}{2}\frac{\sqrt{-\mathfrak{G}}\tan\left(\frac{1}{2}\sqrt{-\mathfrak{G}}\,\mathfrak{Z}\right)}{r}\right)}\right), \tag{46}$$

$$s_{3,2}(x,y,t)=e^{i\psi}\left(-\frac{1}{2}b_1q+\frac{1}{2}\frac{b_1\mathfrak{G}\left(1+\left(\cot\left(\frac{1}{2}\sqrt{-\mathfrak{G}}\,\mathfrak{Z}\right)\right)^2\right)}{q+\sqrt{-\mathfrak{G}}\cot\left(\frac{1}{2}\sqrt{-\mathfrak{G}}\,\mathfrak{Z}\right)}-\frac{b_1p}{\left(-\frac{1}{2}\frac{q}{r}-\frac{1}{2}\frac{\sqrt{-\mathfrak{G}}\cot\left(\frac{1}{2}\sqrt{-\mathfrak{G}}\,\mathfrak{Z}\right)}{r}\right)}\right), \tag{47}$$

$$s_{3,3}(x,y,t)=e^{i\psi}\left(\frac{-b_1\mathfrak{G}(1+\sin(\sqrt{-\mathfrak{G}}\,\mathfrak{Z}))}{\cos(\sqrt{-\mathfrak{G}}\,\mathfrak{Z})(-q\cos(\sqrt{-\mathfrak{G}}\,\mathfrak{Z})+\sqrt{-\mathfrak{G}}\sin(\sqrt{-\mathfrak{G}}\,\mathfrak{Z})+\sqrt{-\mathfrak{G}})}\right.$$
$$\left.-b_1p\left(-\frac{1}{2}\frac{q}{r}+\frac{1}{2}\frac{\sqrt{-\mathfrak{G}}(\tan(\sqrt{-\mathfrak{G}}\,\mathfrak{Z})+\sec(\sqrt{-\mathfrak{G}}\,\mathfrak{Z}))}{r}\right)^{-1}-\frac{1}{2}b_1q\right), \tag{48}$$

and

$$s_{3,4}(x,y,t)=e^{i\psi}\left(\frac{b_1\mathfrak{G}(\sin(\sqrt{-\mathfrak{G}}\,\mathfrak{Z})-1)}{\cos(\sqrt{-\mathfrak{G}}\,\mathfrak{Z})(-q\cos(\sqrt{-\mathfrak{G}}\,\mathfrak{Z})+\sqrt{-\mathfrak{G}}\sin(\sqrt{-\mathfrak{G}}\,\mathfrak{Z})-\sqrt{-\mathfrak{G}})}\right.$$
$$\left.-b_1p\left(-\frac{1}{2}\frac{q}{r}+\frac{1}{2}\frac{\sqrt{-\mathfrak{G}}(\tan(\sqrt{-\mathfrak{G}}\,\mathfrak{Z})-\sec(\sqrt{-\mathfrak{G}}\,\mathfrak{Z}))}{r}\right)^{-1}-\frac{1}{2}b_1q\right). \tag{49}$$

Cluster 3.2: When $\mathfrak{G} > 0,\ r \neq 0$,

$$s_{3,5}(x,y,t) = e^{i\psi}\left(-\frac{1}{2}b_1 q - \frac{1}{2}\frac{b_1\mathfrak{G}(-1+(\tanh(1/2\sqrt{\mathfrak{G}}\,\mathfrak{Z}))^2)}{q+\sqrt{\mathfrak{G}}\tanh\left(\frac{1}{2}\sqrt{\mathfrak{G}}\,\mathfrak{Z}\right)} - \frac{b_1 p}{\left(-\frac{1}{2}\frac{q}{r} - \frac{1}{2}\frac{\sqrt{\mathfrak{G}}\tanh\left(\frac{1}{2}\sqrt{\mathfrak{G}}\,\mathfrak{Z}\right)}{r}\right)}\right), \tag{50}$$

$$\begin{aligned} s_{3,6}(x,y,t) = e^{i\psi}\Bigg(&\frac{-b_1\mathfrak{G}(-1+i\sinh(\sqrt{\mathfrak{G}}\,\mathfrak{Z}))}{\cosh(\sqrt{\mathfrak{G}}\,\mathfrak{Z})(q\cosh(\sqrt{\mathfrak{G}}\,\mathfrak{Z})+\sqrt{\mathfrak{G}}\sinh(\sqrt{\mathfrak{G}}\,\mathfrak{Z})+i\sqrt{\mathfrak{G}})} \\ &- b_1 p\left(-\frac{1}{2}\frac{q}{r} - \frac{1}{2}\frac{\sqrt{\mathfrak{G}}(\tanh(\sqrt{\mathfrak{G}}\,\mathfrak{Z})+i\operatorname{sech}(\sqrt{\mathfrak{G}}\,\mathfrak{Z}))}{r}\right)^{-1} - \frac{1}{2}b_1 q\Bigg), \end{aligned} \tag{51}$$

$$\begin{aligned} s_{3,7}(x,y,t) = e^{i\psi}\Bigg(&\frac{-b_1\mathfrak{G}(1+i\sinh(\sqrt{\mathfrak{G}}\,\mathfrak{Z}))}{\cosh(\sqrt{\mathfrak{G}}\,\mathfrak{Z})(-q\cosh(\sqrt{\mathfrak{G}}\,\mathfrak{Z})-\sqrt{\mathfrak{G}}\sinh(\sqrt{\mathfrak{G}}\,\mathfrak{Z})+i\sqrt{\mathfrak{G}})} \\ &- b_1 p\left(-\frac{1}{2}\frac{q}{r} - \frac{1}{2}\frac{\sqrt{\mathfrak{G}}(\tanh(\sqrt{\mathfrak{G}}\,\mathfrak{Z})-i\operatorname{sech}(\sqrt{\mathfrak{G}}\,\mathfrak{Z}))}{r}\right)^{-1} - \frac{1}{2}b_1 q\Bigg), \end{aligned} \tag{52}$$

and

$$\begin{aligned} s_{3,8}(x,y,t) = e^{i\psi}\Bigg(&\frac{1}{4} - \frac{b_1\mathfrak{G}\left(2\left(\cosh\left(\frac{1}{4}\sqrt{\mathfrak{G}}\,\mathfrak{Z}\right)\right)^2-1\right)}{\cosh\left(\frac{1}{4}\sqrt{\mathfrak{G}}\,\mathfrak{Z}\right)\sinh\left(\frac{1}{4}\sqrt{\mathfrak{G}}\,\mathfrak{Z}\right)\left(-2q\cosh\left(\frac{1}{4}\sqrt{\mathfrak{G}}\,\mathfrak{Z}\right)\sinh\left(\frac{1}{4}\sqrt{\mathfrak{G}}\,\mathfrak{Z}\right)+\sqrt{\mathfrak{G}}\right)} \\ &- b_1 p\left(-\frac{1}{2}\frac{q}{r} - \frac{1}{4}\frac{\sqrt{\mathfrak{G}}\left(\tanh\left(\frac{1}{4}\sqrt{\mathfrak{G}}\,\mathfrak{Z}\right)-\coth\left(\frac{1}{4}\sqrt{\mathfrak{G}}\,\mathfrak{Z}\right)\right)}{r}\right)^{-1} - \frac{1}{2}b_1 q\Bigg). \end{aligned} \tag{53}$$

Cluster 3.3: When $\mathfrak{G} = 0,\quad q \neq 0$,

$$s_{3,9}(x,y,t) = e^{i\psi}\left(-\frac{1}{2}b_1 q - 2\frac{b_1}{\mathfrak{Z}(q\mathfrak{Z}+2)} + \frac{1}{2}\frac{b_1 q^2\mathfrak{Z}}{q\mathfrak{Z}+2}\right). \tag{54}$$

Cluster 3.4: When $\mathfrak{G} = 0$, in case when $q = p = 0$,

$$s_{3,10}(x,y,t) = -e^{i\psi}\left(\frac{b_1}{\mathfrak{Z}}\right). \tag{55}$$

Cluster 3.5: When $q = m$, $p = lm(l \neq 0)$, and $r = 0$,

$$s_{3,11}(x,y,t) = e^{i\psi}\left(-\frac{1}{2}b_1 m + \frac{b_1 m e^{m\mathfrak{Z}}}{e^{m\mathfrak{Z}}-l} - \frac{b_1 m l}{e^{m\mathfrak{Z}}-l}\right). \tag{56}$$

Cluster 3.6: When $q = m$, $r = lm(l \neq 0)$, and $p = 0$,

$$s_{3,12}(x,y,t) = e^{i\psi}\left(-\frac{1}{2}b_1 m - \frac{b_1 m}{-1+le^{m\mathfrak{Z}}}\right). \tag{57}$$

Cluster 3.7: When $p = 0$, $r \neq 0$, and $q \neq 0$,

$$\begin{aligned} s_{3,13}(x,y,t) = e^{i\psi}\Bigg(&-\frac{1}{2}b_1 q \\ &+ \frac{b_1 q(\sinh(q\mathfrak{Z})-\cosh(q\mathfrak{Z}))}{-\cosh(q\mathfrak{Z})+\sinh(q\mathfrak{Z})-k_2}\Bigg), \end{aligned} \tag{58}$$

and

$$s_{3,14}(x,y,t) = e^{i\psi}\left(-\frac{1}{2}b_1 q + \frac{b_1 q k_2}{\cosh(q\mathfrak{Z})+\sinh(q\mathfrak{Z})+k_2}\right). \tag{59}$$

In the above solutions, $\mathfrak{Z} = \frac{\sigma_2 y^\beta}{\beta} - \frac{(2\rho_2\varrho_2\sigma_2+\rho_3(\varrho_1\sigma_2))t^\delta}{\delta}$, $\psi = \frac{\varrho_1 x^\alpha}{\alpha} + \frac{\varrho_2 y^\beta}{\beta} - \frac{\omega t^\delta}{\delta}$, where ω is defined in (18).

Assuming case 4, we gain the resulting soliton solution clusters for (1).

Cluster 4.1: When $\mathfrak{G} < 0,\ r \neq 0$,

$$s_{4,1}(x,y,t)=e^{i\psi}\left(\frac{1}{2}\Omega q+\Omega p\left(-\frac{1}{2}\frac{q}{r}+\frac{1}{2}\times\frac{\sqrt{-\mathfrak{G}}\tan\left(\frac{1}{2}\sqrt{-\mathfrak{G}}\,\mathfrak{Z}\right)}{r}\right)^{-1}\right), \tag{60}$$

$$s_{4,2}(x,y,t)=e^{i\psi}\left(\frac{1}{2}\Omega q+\Omega p\left(-\frac{1}{2}\frac{q}{r}-\frac{1}{2}\frac{\sqrt{-\mathfrak{G}}\cot\left(\frac{1}{2}\sqrt{-\mathfrak{G}}\,\mathfrak{Z}\right)}{r}\right)^{-1}\right), \tag{61}$$

$$s_{4,3}(x,y,t)=e^{i\psi}\left(\frac{1}{2}\Omega q+\Omega p\left(-\frac{1}{2}\frac{q}{r}+\frac{1}{2}\times\frac{\sqrt{-\mathfrak{G}}\left(\tan\left(\sqrt{-\mathfrak{G}}\,\mathfrak{Z}\right)+\sec\left(\sqrt{-\mathfrak{G}}\,\mathfrak{Z}\right)\right)}{r}\right)^{-1}\right), \tag{62}$$

and

$$s_{4,4}(x,y,t)=e^{i\psi}\left(\frac{1}{2}\Omega q+\Omega p\left(-\frac{1}{2}\frac{q}{r}+\frac{1}{2}\times\frac{\sqrt{-\mathfrak{G}}\left(\tan\left(\sqrt{-\mathfrak{G}}\,\mathfrak{Z}\right)-\sec\left(\sqrt{-\mathfrak{G}}\,\mathfrak{Z}\right)\right)}{r}\right)^{-1}\right). \tag{63}$$

Cluster 4.2: When $\mathfrak{G}>0,\quad r\neq 0$,

$$s_{4,5}(x,y,t)=e^{i\psi}\left(\frac{1}{2}\Omega q+\Omega p\left(-\frac{1}{2}\frac{q}{r}-\frac{1}{2}\times\frac{\sqrt{\mathfrak{G}}\tanh\left(\frac{1}{2}\sqrt{\mathfrak{G}}\,\mathfrak{Z}\right)}{r}\right)^{-1}\right), \tag{64}$$

$$s_{4,6}(x,y,t)=e^{i\psi}\left(\frac{1}{2}\Omega q+\Omega p\left(-\frac{1}{2}\frac{q}{r}-\frac{1}{2}\times\frac{\sqrt{\mathfrak{G}}\left(\tanh\left(\sqrt{\mathfrak{G}}\,\mathfrak{Z}\right)+i\operatorname{sech}\left(\sqrt{\mathfrak{G}}\,\mathfrak{Z}\right)\right)}{r}\right)^{-1}\right), \tag{65}$$

$$s_{4,7}(x,y,t)=e^{i\psi}\left(\frac{1}{2}\Omega q+\Omega p\left(-\frac{1}{2}\frac{q}{r}-\frac{1}{2}\times\frac{\sqrt{\mathfrak{G}}\left(\tanh\left(\sqrt{\mathfrak{G}}\,\mathfrak{Z}\right)-i\operatorname{sech}\left(\sqrt{\mathfrak{G}}\,\mathfrak{Z}\right)\right)}{r}\right)^{-1}\right), \tag{66}$$

and

$$s_{4,8}(x,y,t)=e^{i\psi}\left(\frac{1}{2}\Omega q+\Omega p\left(-\frac{1}{2}\frac{q}{r}-\frac{1}{4}\times\frac{\sqrt{\mathfrak{G}}\left(\tanh\left(\frac{1}{4}\sqrt{\mathfrak{G}}\,\mathfrak{Z}\right)-\coth\left(\frac{1}{4}\sqrt{\mathfrak{G}}\,\mathfrak{Z}\right)\right)}{r}\right)^{-1}\right). \tag{67}$$

Cluster 4.3: When $\mathfrak{G}=0,\quad q\neq 0$,

$$s_{4,9}(x,y,t)=e^{i\psi}\left(\frac{1}{2}\Omega q-\frac{1}{2}\frac{\Omega q^2\mathfrak{Z}}{q\mathfrak{Z}+2}\right). \tag{68}$$

Cluster 4.4: When $\mathfrak{G}=0$, in case when $q=r=0$,

$$s_{4,10}(x,y,t)=e^{i\psi}\left(\frac{\Omega}{\mathfrak{Z}}\right). \tag{69}$$

Cluster 4.5: When $q=m$, $p=lm(l\neq 0)$, and $r=0$,

$$s_{4,11}(x,y,t)=e^{i\psi}\left(\frac{1}{2}\Omega m+\frac{\Omega ml}{e^{m\mathfrak{Z}}-l}\right). \tag{70}$$

Cluster 4.6: When $q=m$, $r=lm(l\neq 0)$, and $p=0$,

$$s_{4,12}(x,y,t)=e^{i\psi}\left(\frac{1}{2}\Omega m\right). \tag{71}$$

Cluster 4.7: When $p=0$, $r\neq 0$, and $q\neq 0$,

$$s_{4,13}(x,y,t)=e^{i\psi}\left(\frac{1}{2}\Omega q\right), \tag{72}$$

In the above solutions, $\mathfrak{Z}=\frac{\sigma_1x^{\alpha}}{\alpha}+\frac{\sigma_2y^{\beta}}{\beta}-\frac{(2\rho_1\varrho_1\sigma_1+2\rho_2\varrho_2\sigma_2+\varrho_2\sigma_1+\rho_3(\varrho_1\sigma_2))t^{\delta}}{\delta}$, $\psi=\frac{\varrho_1x^{\alpha}}{\alpha}+\frac{\varrho_2y^{\beta}}{\beta}-\frac{\omega t^{\delta}}{\delta}$, where ω is defined in (19).

Assuming case 5, we gain the resulting soliton solution clusters for (1).

Cluster 5.1: When $\mathfrak{G}<0,\quad r\neq 0$,

$$s_{5,1}(x,y,t)=e^{i\psi}\left(b_0-\frac{1}{2}\frac{b_1\mathfrak{G}\left(1+\left(\tan\left(\frac{1}{2}\sqrt{-\mathfrak{G}}\,\mathfrak{Z}\right)\right)^2\right)}{-q+\sqrt{-\mathfrak{G}}\tan\left(\frac{1}{2}\sqrt{-\mathfrak{G}}\,\mathfrak{Z}\right)}+a_0\left(-\frac{1}{2}\frac{q}{r}+\frac{1}{2}\frac{\sqrt{-\mathfrak{G}}\tan\left(\frac{1}{2}\sqrt{-\mathfrak{G}}\,\mathfrak{Z}\right)}{r}\right)^{-1}\right), \tag{73}$$

$$s_{5,2}(x,y,t)=e^{i\psi}\left(b_0+\frac{1}{2}\frac{b_1\mathfrak{G}\left(1+\left(\cot\left(\frac{1}{2}\sqrt{-\mathfrak{G}}\,\mathfrak{Z}\right)\right)^2\right)}{q+\sqrt{-\mathfrak{G}}\cot\left(\frac{1}{2}\sqrt{-\mathfrak{G}}\,\mathfrak{Z}\right)}+a_0\left(-\frac{1}{2}\frac{q}{r}-\frac{1}{2}\frac{\sqrt{-\mathfrak{G}}\cot\left(\frac{1}{2}\sqrt{-\mathfrak{G}}\,\mathfrak{Z}\right)}{r}\right)^{-1}\right), \tag{74}$$

$$s_{5,3}(x,y,t) = e^{i\psi}\left(\frac{-b_1\mathfrak{G}(1+\sin(\sqrt{-\mathfrak{G}}\,\mathfrak{Z}))}{\cos(\sqrt{-\mathfrak{G}}\,\mathfrak{Z})(-q\cos(\sqrt{-\mathfrak{G}}\,\mathfrak{Z})+\sqrt{-\mathfrak{G}}\,\sin(\sqrt{-\mathfrak{G}}\,\mathfrak{Z})+\sqrt{-\mathfrak{G}})} + a_0\left(-\frac{1}{2}\frac{q}{r}+\frac{1}{2}\frac{\sqrt{-\mathfrak{G}}(\tan(\sqrt{-\mathfrak{G}}\,\mathfrak{Z})+\sec(\sqrt{-\mathfrak{G}}\,\mathfrak{Z}))}{r}\right)^{-1}+b_0\right), \tag{75}$$

and

$$s_{5,4}(x,y,t) = e^{i\psi}\left(\frac{b_1\mathfrak{G}(\sin(\sqrt{-\mathfrak{G}}\,\mathfrak{Z})-1)}{\cos(\sqrt{-\mathfrak{G}}\,\mathfrak{Z})(-q\cos(\sqrt{-\mathfrak{G}}\,\mathfrak{Z})+\sqrt{-\mathfrak{G}}\,\sin(\sqrt{-\mathfrak{G}}\,\mathfrak{Z})-\sqrt{-\mathfrak{G}})} + a_0\left(-\frac{1}{2}\frac{q}{r}+\frac{1}{2}\frac{\sqrt{-\mathfrak{G}}(\tan(\sqrt{-\mathfrak{G}}\,\mathfrak{Z})-\sec(\sqrt{-\mathfrak{G}}\,\mathfrak{Z}))}{r}\right)^{-1}+b_0\right). \tag{76}$$

Cluster 5.2: When $\mathfrak{G} > 0,\ r \neq 0$,

$$s_{5,5}(x,y,t) = e^{i\psi}\left(b_0 - \frac{1}{2}\frac{b_1\mathfrak{G}\left(-1+\left(\tanh\left(\frac{1}{2}\sqrt{\mathfrak{G}}\,\mathfrak{Z}\right)\right)^2\right)}{q+\sqrt{\mathfrak{G}}\tanh\left(\frac{1}{2}\sqrt{\mathfrak{G}}\,\mathfrak{Z}\right)} + a_0\left(-\frac{1}{2}\frac{q}{r}-\frac{1}{2}\frac{\sqrt{\mathfrak{G}}\tanh\left(\frac{1}{2}\sqrt{\mathfrak{G}}\,\mathfrak{Z}\right)}{r}\right)^{-1}\right), \tag{77}$$

$$s_{5,6}(x,y,t) = e^{i\psi}\left(\frac{-b_1\mathfrak{G}(-1+i\sinh(\sqrt{\mathfrak{G}}\,\mathfrak{Z}))}{\cosh(\sqrt{\mathfrak{G}}\,\mathfrak{Z})(q\cosh(\sqrt{\mathfrak{G}}\,\mathfrak{Z})+\sqrt{\mathfrak{G}}\,\sinh(\sqrt{\mathfrak{G}}\,\mathfrak{Z})+i\sqrt{\mathfrak{G}})} + a_0\left(-\frac{1}{2}\frac{q}{r}-\frac{1}{2}\frac{\sqrt{\mathfrak{G}}(\tanh(\sqrt{\mathfrak{G}}\,\mathfrak{Z})+i\mathrm{sech}(\sqrt{\mathfrak{G}}\,\mathfrak{Z}))}{r}\right)^{-1}+b_0\right), \tag{78}$$

$$s_{5,7}(x,y,t) = e^{i\psi}\left(\frac{-b_1\mathfrak{G}(1+i\sinh(\sqrt{\mathfrak{G}}\,\mathfrak{Z}))}{\cosh(\sqrt{\mathfrak{G}}\,\mathfrak{Z})(-q\cosh(\sqrt{\mathfrak{G}}\,\mathfrak{Z})-\sqrt{\mathfrak{G}}\,\sinh(\sqrt{\mathfrak{G}}\,\mathfrak{Z})+i\sqrt{\mathfrak{G}})} + a_0\left(-\frac{1}{2}\frac{q}{r}-\frac{1}{2}\frac{\sqrt{\mathfrak{G}}(\tanh(\sqrt{\mathfrak{G}}\,\mathfrak{Z})-i\mathrm{sech}(\sqrt{\mathfrak{G}}\,\mathfrak{Z}))}{r}\right)^{-1}+b_0\right), \tag{79}$$

and

$$s_{5,8}(x,y,t) = e^{i\psi}\left(\frac{-b_1\mathfrak{G}\left(2\left(\cosh\left(\frac{1}{4}\sqrt{\mathfrak{G}}\,\mathfrak{Z}\right)\right)^2-1\right)}{4\cosh\left(\frac{1}{4}\sqrt{\mathfrak{G}}\,\mathfrak{Z}\right)\sinh\left(\frac{1}{4}\sqrt{\mathfrak{G}}\,\mathfrak{Z}\right)\left(-2q\cosh\left(\frac{1}{4}\sqrt{\mathfrak{G}}\,\mathfrak{Z}\right)\sinh\left(\frac{1}{4}\sqrt{\mathfrak{G}}\,\mathfrak{Z}\right)+\sqrt{\mathfrak{G}}\right)} + a_0\left(-\frac{1}{2}\frac{q}{r}-\frac{1}{4}\frac{\sqrt{\mathfrak{G}}\left(\tanh\left(\frac{1}{4}\sqrt{\mathfrak{G}}\,\mathfrak{Z}\right)-\coth\left(\frac{1}{4}\sqrt{\mathfrak{G}}\,\mathfrak{Z}\right)\right)}{r}\right)^{-1}+b_0\right). \tag{80}$$

Cluster 5.3: When $\mathfrak{G} = 0,\ q \neq 0$,

$$s_{5,9}(x,y,t) = e^{i\psi}\left(b_0 - 2\frac{b_1}{\mathfrak{Z}(q\mathfrak{Z}+2)} - \frac{1}{2}\frac{a_0q^2\mathfrak{Z}}{p(q\mathfrak{Z}+2)}\right). \tag{81}$$

Cluster 5.4: When $\mathfrak{G} = 0$, in case when $q = r = 0$,

$$s_{5,10}(x,y,t) = e^{i\psi}\left(b_0 + \frac{b_1}{\mathfrak{Z}} + \frac{a_0}{p\mathfrak{Z}}\right). \tag{82}$$

Cluster 5.5: When $\mathfrak{G} = 0$, in case when $q = p = 0$,

$$s_{5,11}(x,y,t) = e^{i\psi}\left(b_0 - \frac{b_1}{\mathfrak{Z}} - a_0r\mathfrak{Z}\right). \tag{83}$$

Cluster 5.6: When $q = m,\ p = lm(l \neq 0)$, and $r = 0$,

$$s_{5,12}(x,y,t) = e^{i\psi}\left(b_0 + \frac{b_1me^{m\mathfrak{Z}}}{e^{m\mathfrak{Z}}-l} + \frac{a_0}{e^{m\mathfrak{Z}}-l}\right). \tag{84}$$

Cluster 5.7: When $q = m,\ r = lm(l \neq 0)$, and $p = 0$,

$$s_{5,13}(x,y,t) = e^{i\psi}\left(b_0 - \frac{b_1m}{-1+le^{m\mathfrak{Z}}} + \frac{a_0(1-le^{m\mathfrak{Z}})}{e^{m\mathfrak{Z}}}\right). \tag{85}$$

Cluster 5.8: When $p = 0$, $r \neq 0$, and $q \neq 0$,

$$s_{5,14}(x, y, t) = e^{i\psi}\left(b_0 + \frac{b_1 q(\sinh(q\mathfrak{Z}) - \cosh(q\mathfrak{Z}))}{-\cosh(q\mathfrak{Z}) + \sinh(q\mathfrak{Z}) - k_2} - \frac{a_0 r(\cosh(q\mathfrak{Z}) - \sinh(q\mathfrak{Z}) + k_2)}{k_1 q}\right) \tag{86}$$

and

$$s_{5,15}(x, y, t) = e^{i\psi}\left(b_0 + \frac{b_1 q k_2}{\cosh(q\mathfrak{Z}) + \sinh(q\mathfrak{Z}) + k_2} - \frac{a_0 r(\cosh(q\mathfrak{Z}) + \sinh(q\mathfrak{Z}) + k_2)}{q(\cosh(q\mathfrak{Z}) + \sinh(q\mathfrak{Z}))}\right). \tag{87}$$

In the above solutions, $\mathfrak{Z} = \frac{\sigma_1 x^\alpha}{\alpha} - \frac{(2\rho_1 \varrho_1 \sigma_1 + \varrho_2 \sigma_1)t^\delta}{\delta}$, $\psi = \frac{\varrho_1 x^\alpha}{\alpha} + \frac{\varrho_2 y^\beta}{\beta} - \frac{\omega t^\delta}{\delta}$, where ω is defined in (20).

4 Discussion and graphs

This section provides a more thorough analysis of the solitons' dynamical behavior as seen in CHFSCE. Using RMESEM, we obtain these soliton solutions, allowing us to fully comprehend the intricate dynamics of the CHFSCE. By varying the model's parameter values, we were able to generate several 2D, 3D, and contour graphs that demonstrated the wave behavior of the resulting soliton solutions. These graphs show how wave amplitudes and spatial characteristics are related and may be used to investigate several profiles found in the solution. These depictions show the solitonic phenomena, including fractal, internal envelope, periodic, multiple periodic, parabolic, and hump solitons, by emphasizing the corporeal aspect of periodic oscillations in the solitons. Every profile is distinct from others and provides important information on the underlying dynamics of the CHFSCE system.

Since this technique has never been used for the CHFSCE before, the findings of this study are revolutionary. Because RMESEM is a simple algebraic ansatz that does not involve complex procedures like linearization, perturbation, and other transformation techniques – which are sometimes necessary in other approaches – we have specifically chosen it. We can obtain accurate closed-form responses without the headaches of more complicated methods thanks to RMESEM's simplicity and effectiveness. One of RMESEM's primary characteristics is its ability to offer a wide range of solution families, including exponential, rational, hyperbolic, and trigonometric functions, among others. This variation enables a more comprehensive analysis of the model by revealing a broad range of wave characteristics that other methods could overlook or be unable to capture. RMESEM offers a variety of solution forms in contrast to more conventional methods, allowing for a deeper and more comprehensive understanding of the dynamics inherent in the model under study. It should be mentioned, nonetheless, that the suggested approach is useless if the greatest nonlinear component and the highest derivative terms do not balance uniformly. Due to the method's inability to balance the nonlinear component with dispersion, soliton generation is not possible in this scenario. Notwithstanding this limitation, the present investigation demonstrates that the methodology employed in this work is very dependable and efficient for nonlinear problems in a range of scientific domains.

4.1 Dynamics of $s(x, y, t)$

Inside CHFSCE, graphs for obtained complex soliton solutions $s(x, y, t)$ clearly show quasi-periodic such as smooth-periodic, multiple periodic, and periodic-periodic soliton phenomena. The emergence of fractal geometries in the aimed model can be attributed to various factors, such as the existence of periodic solitons, the fractional derivative, the nonlinearity, and soliton interactions in the context of CHFSCE. Periodic oscillations in solitons can be responsible for the creation of fractals because they cause self-similarities at different sizes. The CFD may also be responsible for the emergence of fractals since noninteger spin values introduces scaling symmetries which are hallmark of fractal structures since this similarity also allows for patterns that are self-similar in pattern which emerge at different scales. The combination of fractional derivative with nonlinear terms can lead to chaotic behavior in the system, due to which fractal may arise. In some profiles, periodic soliton were found in interaction with internal envelope soliton. The phenomenon of soliton amplitude modulations caused by each additional structure that forms in the primary soliton is referred to as the internal envelope soliton. The presence of periodic and internal envelope soliton might provide important information about the stability, phase transitions, interactions, disorders, and complexity of magnetic spins. Such solitons draw attention to the rich dynamics at work and imply that the interactions between the solitons may result in complicated and chaotic behaviors that are essential for comprehending the dynamics of the system as a whole. These occurrences imply different levels of stability and complexity because of the effect of the fractional derivative involved. Various other information can be encoded in fractal soliton structures, such as the spatial distribution to the spin correlation (providing

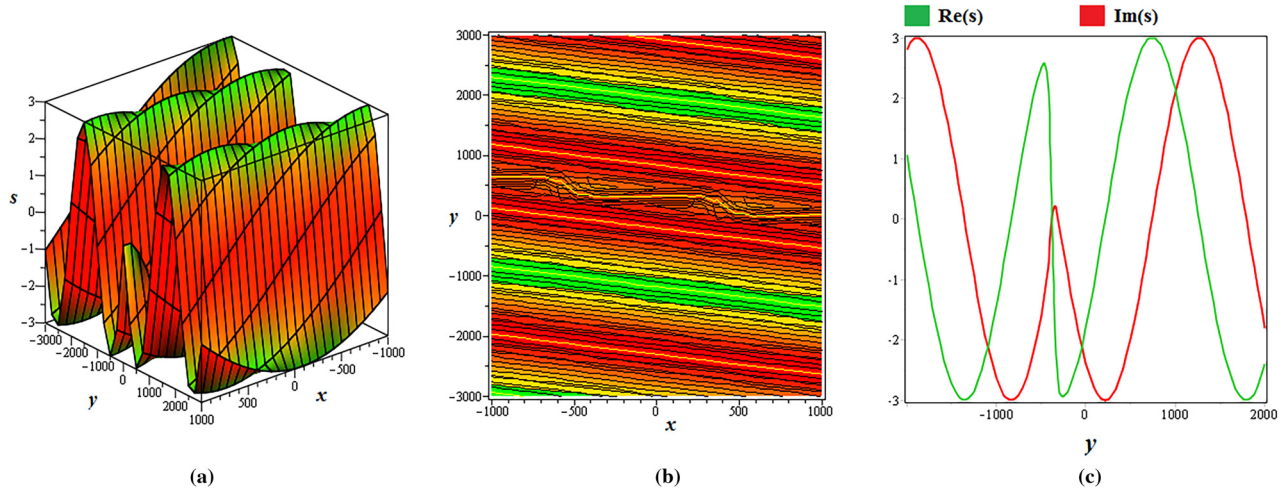

Figure 1: These 3D, contour, and 2D (when x = 2,000) visuals for apart periodic-periodic soliton solutions $s_{1,5}(x, y, t)$ in (25) are sketched when p = 1, q = 5, r = 4, $\varrho_1 = 0.1E^{-2}$, $\varrho_2 = 0.3E^{-2}$, $\sigma_1 = 0.5E^{-2}$, $\sigma_2 = 0.15E^{-1}$, κ_1 = 1, κ_2 = 2, α = 1, β = 1, δ = 1, t = 1, a_0 = 2, B = 3, and ν = 1.

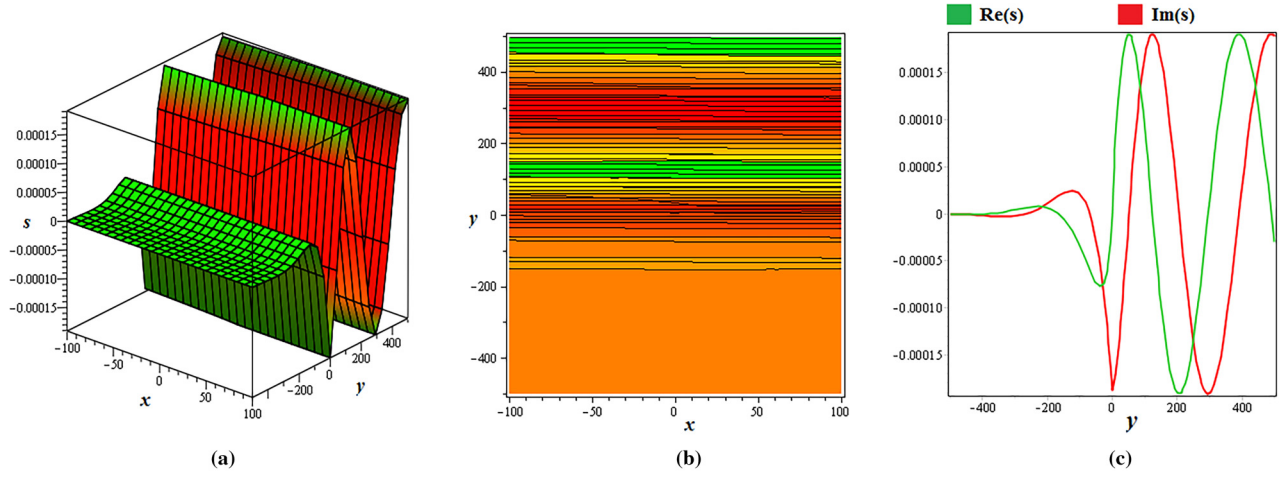

Figure 2: These 3D, contour, and 2D (when x = 100) visuals for smooth-periodic soliton solutions $s_{1,9}(x, y, t)$ in (29) are sketched when p = 1, q = 2, r = 1, $\varrho_1 = 0.1E^{-2}$, $\varrho_2 = 0.53E^{-1}$, $\sigma_1 = 0.45E^{-1}$, $\sigma_2 = 0.225E^{-1}$, κ_1 = 1, κ_2 = 4, α = 0.7, β = 0.8, δ = 0.9, t = 100, a_0 = 1, B = 2, and ν = 5.

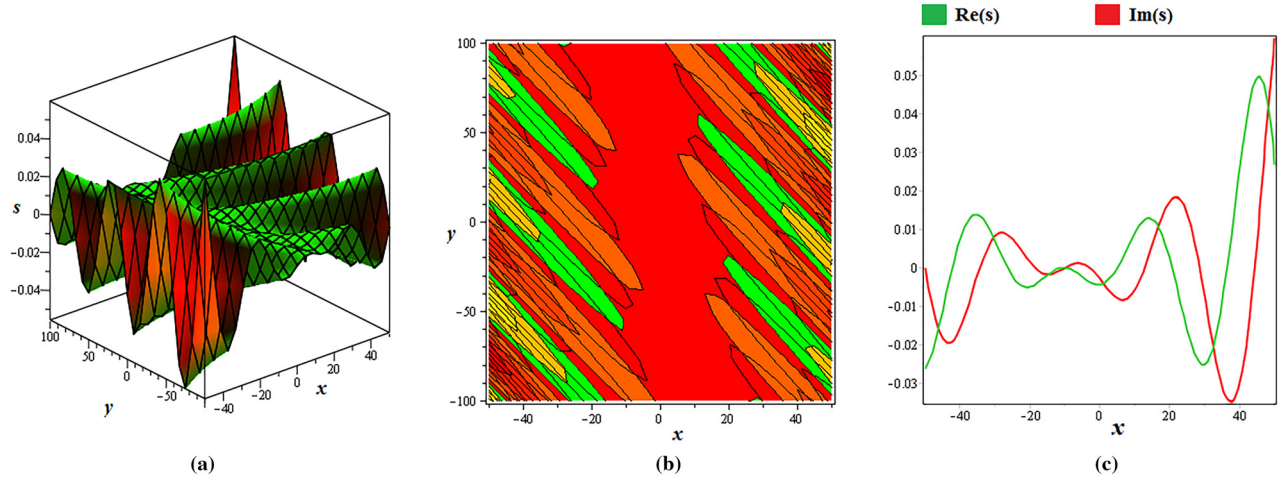

Figure 3: These 3D, contour, and 2D (when y = 100) visuals for double-periodic soliton solutions $s_{2,1}(x, y, t)$ in (32) are sketched when p = 4, q = 0, r = 1, ϱ_1 = 0.2, ϱ_2 = 0.1, $\sigma_1 = 0.1E^{-1}$, $\sigma_2 = 0.1E^{-2}$, κ_1 = 2, κ_2 = 0.5, α = 1, β = 1, δ = 0.5, t = 0, B = 1, ν = 2, and κ = 1.

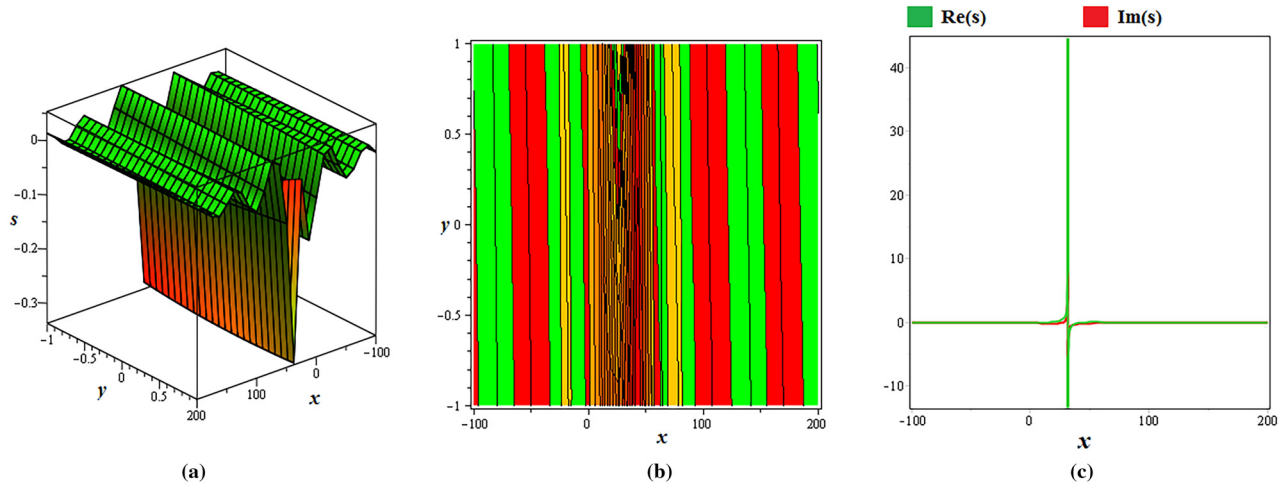

Figure 4: These 3D, contour, and 2D (when $y = 0$) visuals for internal envelope-periodic soliton solutions $s_{2,10}(x, y, t)$ in (41) are sketched when $p = 0$, $q = 0$, $r = 5$, $\varrho_1 = 0.1$, $\varrho_2 = 0.2$, $\sigma_1 = 0.5$, $\sigma_2 = 0.3$, $\kappa_1 = 1$, $\kappa_2 = 2$, $\alpha = 1$, $\beta = 1$, $\delta = 1$, $t = 10$, $B = 2$, $\nu = 1$, and $\kappa = 5$.

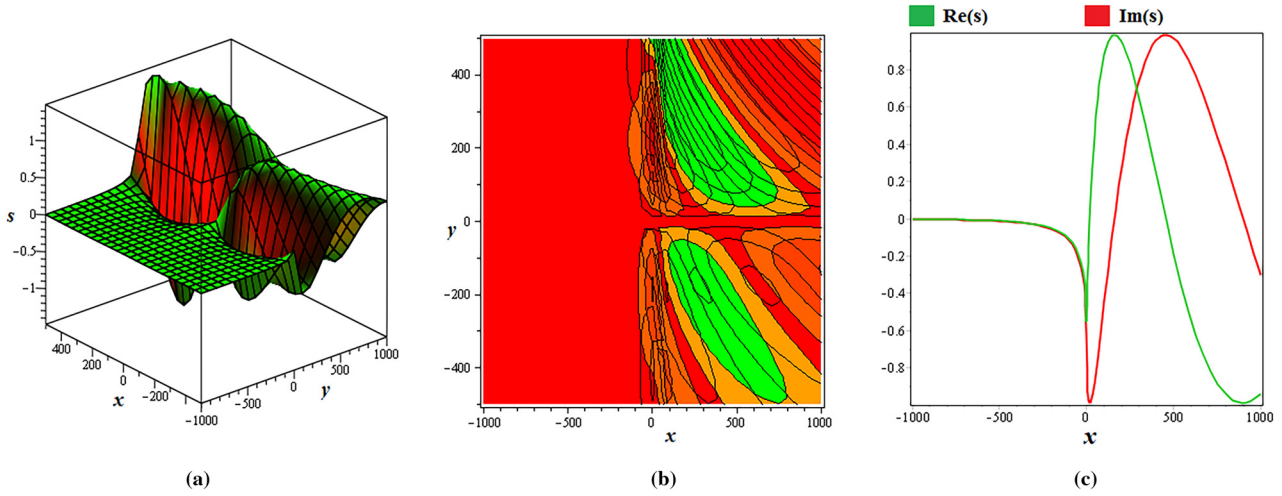

Figure 5: These 3D, contour, and 2D (when $y = 100$) visuals for perturbed-periodic soliton solutions $s_{3,5}(x, y, t)$ in (50) are sketched when $p = 1, q = 5$, $r = 4$, $\varrho_1 = 0.91E^{-1}$, $\varrho_2 = 0.12E^{-1}$, $\sigma_1 = 0$, $\sigma_2 = 0.75E^{-2}$, $\kappa_2 = 1$, $\alpha = 0.5$, $\beta = 0.9$, $\delta = 0.1$, $t = 0$, $B = 1$, $\nu = 2$, $\kappa = 5$, and $b_1 = 1$.

valuable insight into the magnetic ordering/disordering of the system), critical behavior by indicating proximity to critical points, describing system's energy distribution (revealing the information about energy maxima and minima), quantum computing (since fractals may be relevant to it particularly in the realm of many-body localization and quantum spin chain) and dynamical properties such as relaxation rate, propagation, and thermal conductivity of spin-wave propagation.

Moreover, Figure 1 corresponds to $s_{1,5}(x, y, t)$ presented in (25), which forms fractal soliton profile due to the propagation of apart periodic-periodic solitons. Figure 2 corresponds to $s_{1,9}(x, y, t)$ presented in (29), which forms fractal soliton profile due to the propagation of smooth-periodic soliton. Figure 3 corresponds to $s_{2,1}(x, y, t)$ presented in (32), which forms fractal soliton profile due to the propagation of double-periodic soliton. Figure 4 corresponds to $s_{2,10}(x, y, t)$ presented in (41), which forms fractal soliton profile due to the propagation of internal envelope-periodic soliton. Figure 5 corresponds to $s_{3,5}(x, y, t)$ presented in (50), which forms fractal soliton profile due to the propagation of perturbed-periodic soliton. Figure 6 corresponds to $s_{3,9}(x, y, t)$ presented in (54), which forms fractal soliton profile due to the propagation of smooth-periodic soliton. Figure 7 corresponds to $s_{4,10}(x, y, t)$ presented in (69), which forms fractal soliton profile due to the propagation of breather type internal envelope-periodic soliton. Figure 8 corresponds to $s_{4,13}(x, y, t)$ presented in (72), which

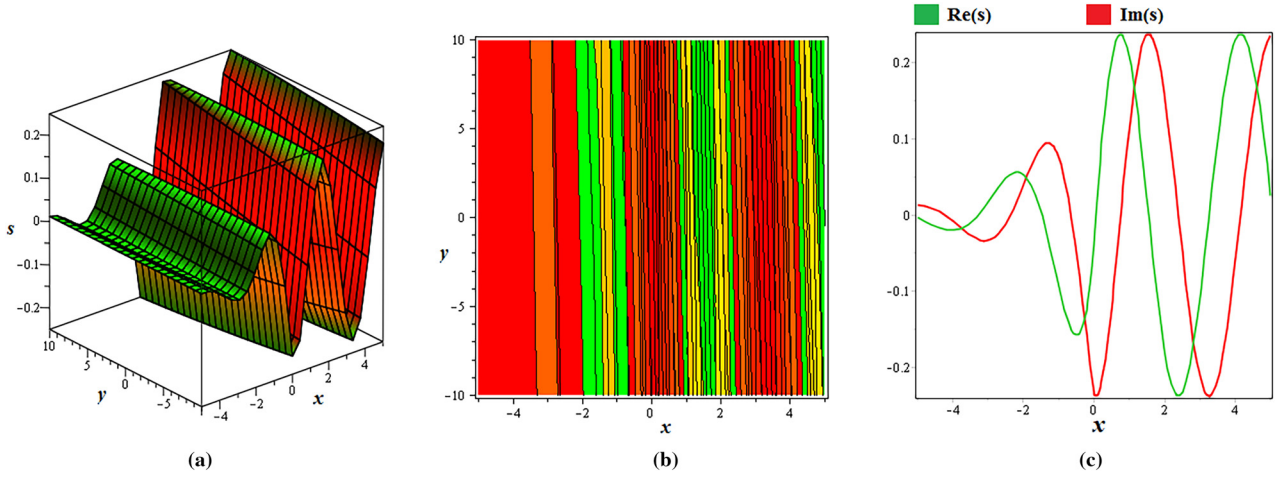

Figure 6: These 3D, contour, and 2D (when $y = 1$) visuals for smooth-periodic soliton solution $s_{3,9}(x, y, t)$ in (54) are sketched when $p = 2$, $q = 4$, $r = 2$, $\varrho_1 = 2$, $\varrho_2 = 0.2E^{-1}$, $\sigma_1 = 0$, $\sigma_2 = 0.5E^{-1}$, $\kappa_2 = 2$, $\alpha = 0.9$, $\beta = 1$, $\delta = 0.8$, $t = 1$, $B = 2$, $\nu = 1$, $\kappa = 0.5$, and $b_1 = 2$.

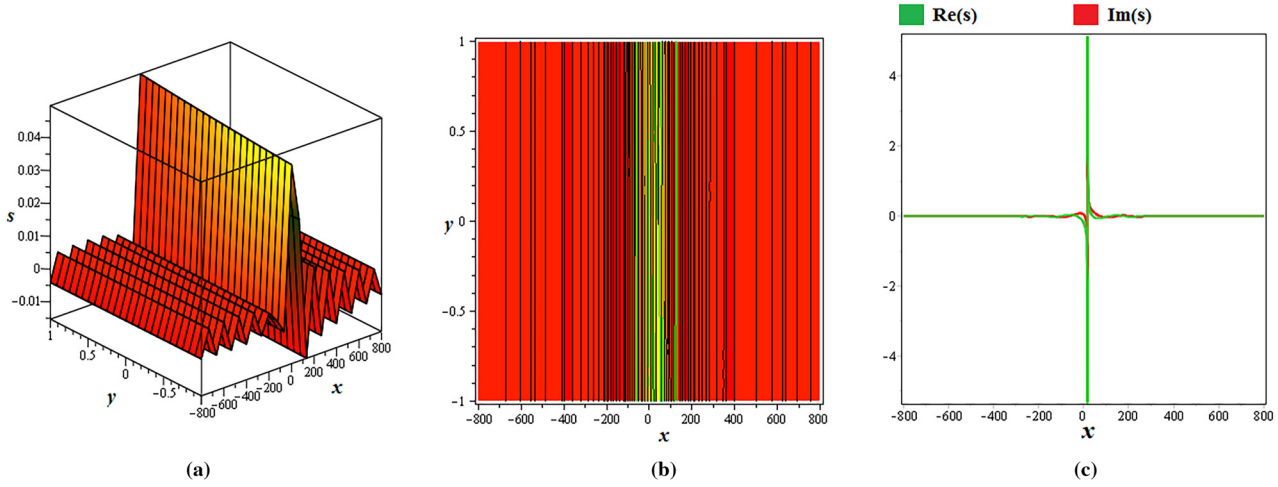

Figure 7: These 3D, contour, and 2D (when $y = 0$) visuals for internal envelope-periodic soliton solutions $s_{4,10}(x, y, t)$ in (69) are sketched when $p = 5$, $q = 0$, $r = 0$, $\varrho_1 = 0.45E^{-1}$, $\varrho_2 = 0.15E^{-1}$, $\sigma_1 = 0.35E^{-1}$, $\sigma_2 = 0.65E^{-1}$, $\kappa_1 = 3$, $\kappa_2 = 1$, $\alpha = 1$, $\beta = 1$, $\delta = 0.5$, $t = 100$, $B = 2$, $\nu = 1$, and $\kappa = 4$.

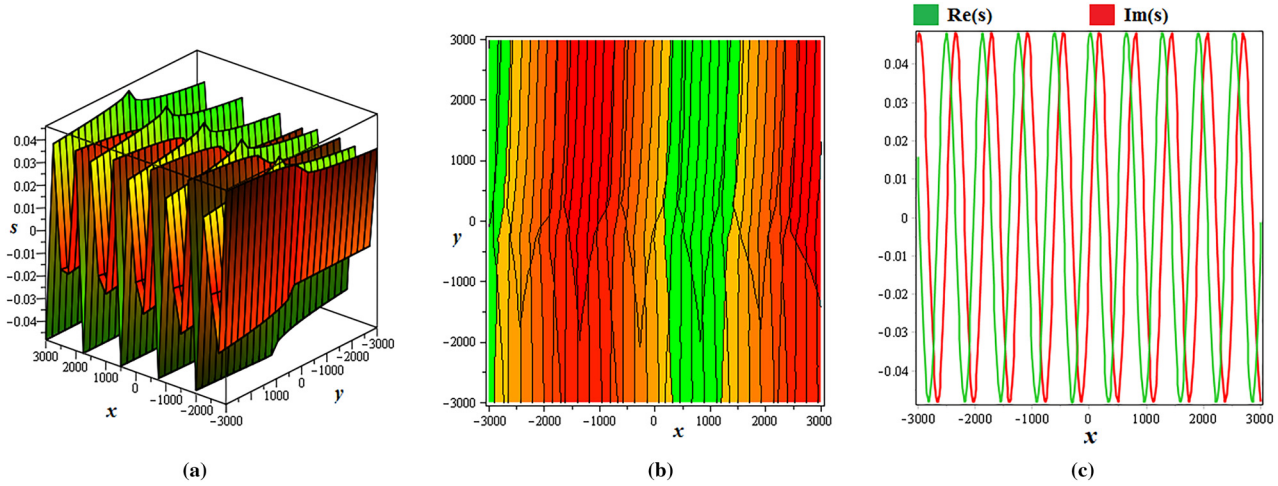

Figure 8: These 3D, contour, and 2D (when $y = 3{,}000$) visuals for double-periodic soliton solutions $s_{4,13}(x, y, t)$ in (72) are sketched when $p = 0, q = 1$, $r = 3$, $\varrho_1 = 0.1E^{-1}$, $\varrho_2 = 0.5E^{-2}$, $\sigma_1 = 0.3E^{-1}$, $\sigma_2 = 0.175E^{-1}$, $\kappa_1 = 1$, $\kappa_2 = 2$, $\alpha = 1$, $\beta = 0.4$, $\delta = 0.3$, $t = 5$, $B = 1$, $\nu = 2$, $\kappa = 5$, and $k_2 = 2$.

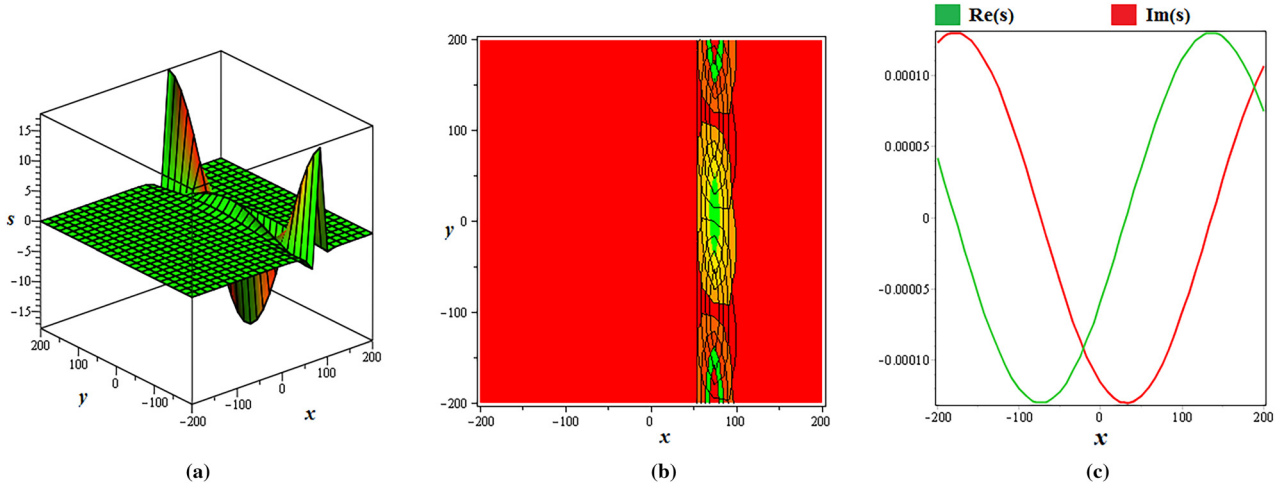

Figure 9: These 3D, contour, and 2D (when $x = 200$) visuals for double-periodic soliton solutions $s_{5,8}(x, y, t)$ in (80) are sketched when $p = 8, q = 10$, $r = 2, \varrho_1 = 0.22E^{-1}, \varrho_2 = 0.15E^{-1}, \sigma_1 = 0.25E^{-1}, \sigma_2 = 0, \kappa_1 = 5, \kappa_2 = 1, \alpha = 1, \beta = 1, \delta = 0.3, t = 20, B = 0, \nu = 3, \kappa = 1, b_0 = 2, b_1 = 1$, and $a_0 = 5$.

forms fractal soliton profile due to the propagation of degenerated double-periodic soliton. Figure 9 corresponds to $s_{5,8}(x, y, t)$ presented in (80), which forms fractal soliton profile due to the propagation of double-periodic soliton. Figure 10 corresponds to $s_{5,12}(x, y, t)$ presented in (84), which forms fractal soliton profile due to the propagation of multiple-periodic soliton.

4.2 Dynamics of $|s(x, y, t)|^2$

In the domain of CHFSCE, the graphs for the squared norms $|s(x, y, t)|^2$ of the obtained soliton solutions show hump, corresponding to dark and bright soliton, peakon, and parabolic soliton phenomena. Because of the localized drop in the soliton amplitude, dark hump solitons are identifiable by them. This soliton phenomena can be related to the areas where magnetic spin decreases, which would suggest a localized spin density depletion area or a zone of destructive interference. In contrast, bright solitons are characterized by a concentrated peak or rise in amplitude that results in a hump in the waveforms. Unlike dark solitons, this soliton is representative of the areas where the magnetic spin density rises and the interactions between the particles result in a coherent state that propagates without dissipating. To sum up, these soliton occurrences are distinct states of the magnetic spin density. Peakon on the other hand is a soliton with a sharp peak. Finally parabolic soliton is a soliton with parabolic structure. A compacton parabolic is a parabolic soliton with compact

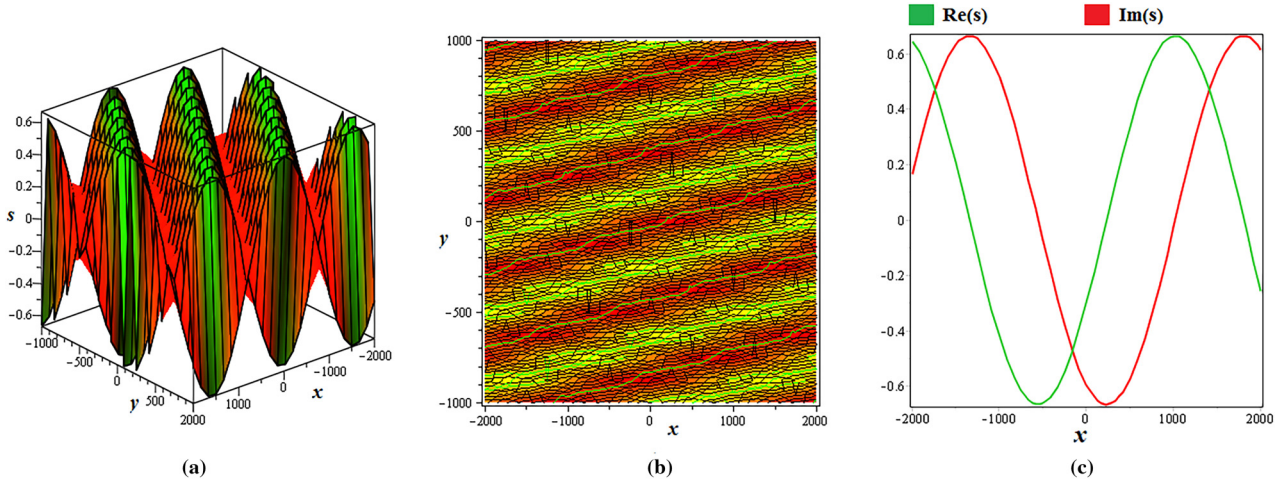

Figure 10: These 3D, contour, and 2D (when $y = 0$) visuals for multiple-periodic soliton solutions $s_{5,12}(x, y, t)$ in (84) are sketched when $m = 2, l = 3$, $p = ml, q = m, r = 0, \varrho_1 = 0.2E^{-2}, \varrho_2 = 0.35E^{-1}, \sigma_1 = 0.135E^{-1}, \sigma_2 = 0, \kappa_1 = 2, \kappa_2 = 3, \alpha = 1, \beta = 1, \delta = 8, t = 10, B = 0, \nu = 2, \kappa = 2, b_0 = 1, b_1 = 5$, and $a_0 = 1$.

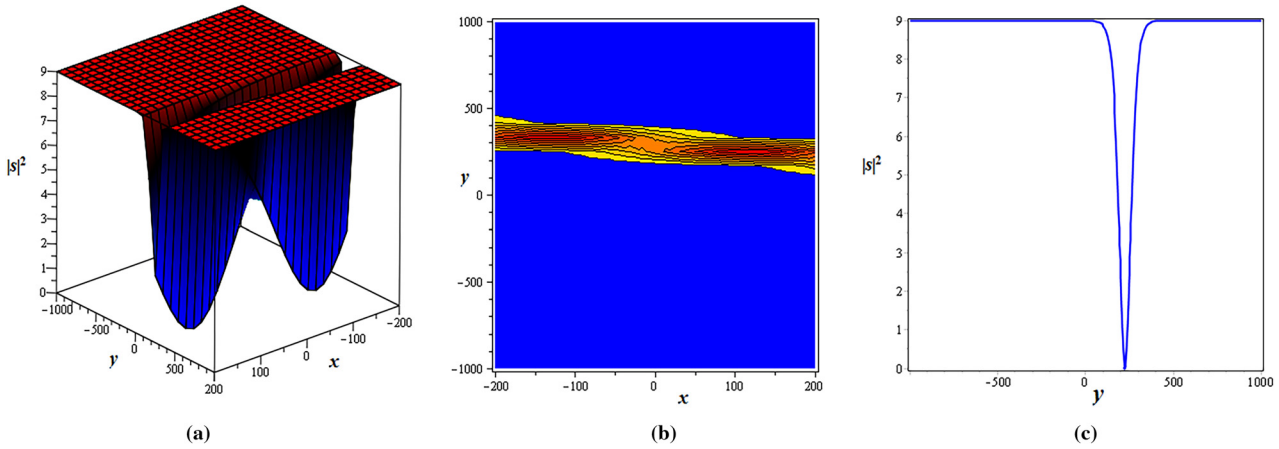

Figure 11: These 3D, contour, and 2D (when $x = 200$) visuals for squared norm $|s|^2$ of the soliton solutions $s_{1,5}(x, y, t)$ in (25) are sketched when $p = 1$, $q = 5$, $r = 4$, $\varrho_1 = 0.1E^{-2}$, $\varrho_2 = 0.3E^{-2}$, $\sigma_1 = 0.5E^{-2}$, $\sigma_2 = 0.15E^{-1}$, $\kappa_1 = 1$, $\kappa_2 = 2$, $\alpha = 1$, $\beta = 1$, $\delta = 1$, $t = 1$, $a_0 = 2$, $B = 3$, and $\nu = 1$.

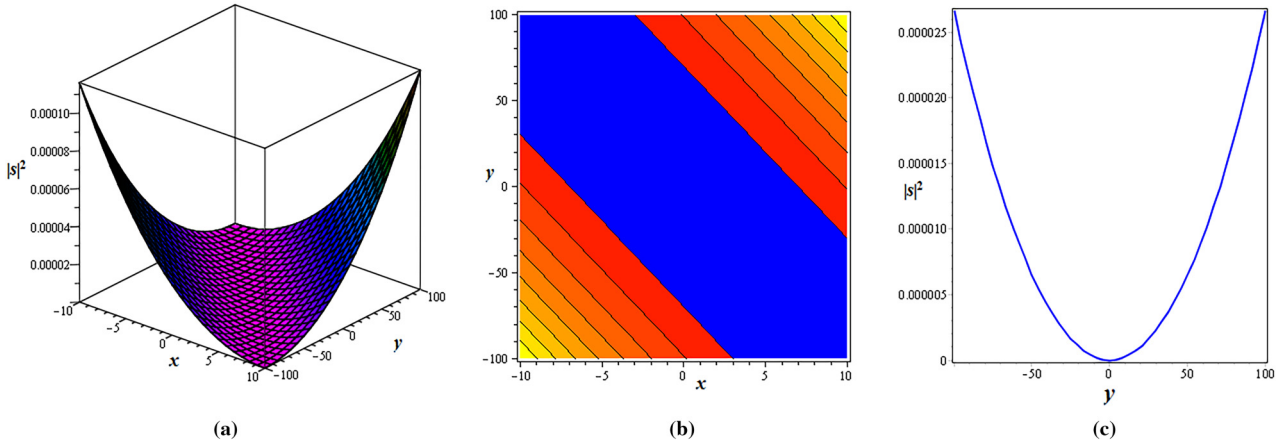

Figure 12: These 3D, contour, and 2D (when $x = 0$) visuals for squared norm $|s|^2$ of the soliton solution $s_{2,1}(x, y, t)$ in (32) are sketched when $p = 4$, $q = 0$, $r = 1$, $\varrho_1 = 0.2$, $\varrho_2 = 0.1$, $\sigma_1 = 0.1E^{-1}$, $\sigma_2 = 0.1E^{-2}$, $\kappa_1 = 2$, $\kappa_2 = 0.5$, $\alpha = 1$, $\beta = 1$, $\delta = 0.5$, $t = 0$, $B = 1$, $\nu = 2$, and $\kappa = 1$.

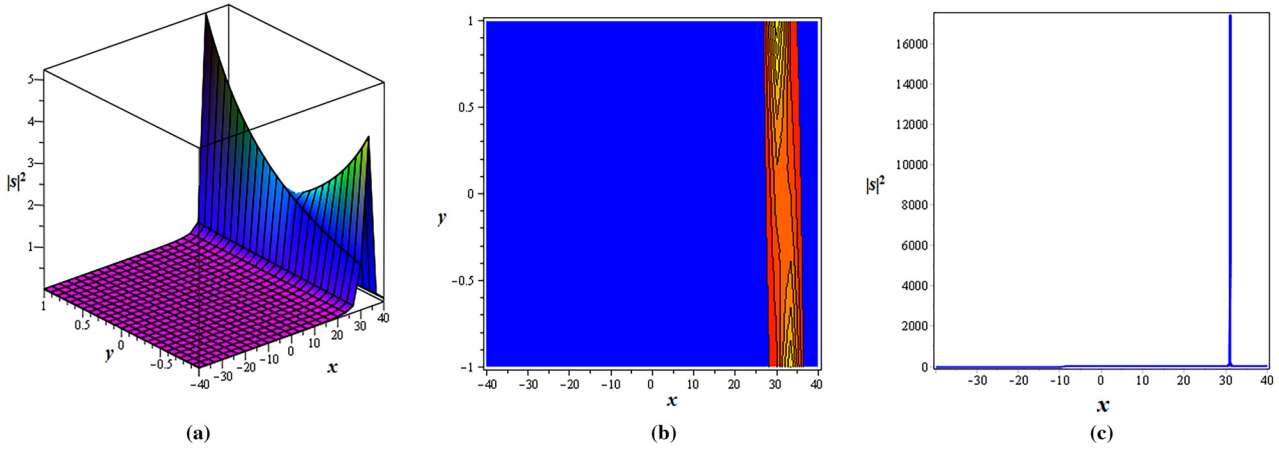

Figure 13: These 3D, contour, and 2D (when $y = 1$) visuals for squared norm $|s|^2$ of the soliton solutions $s_{2,10}(x, y, t)$ in (41) are sketched when $p = 0$, $q = 0$, $r = 5$, $\varrho_1 = 0.1$, $\varrho_2 = 0.2$, $\sigma_1 = 0.5$, $\sigma_2 = 0.3$, $\kappa_1 = 1$, $\kappa_2 = 2$, $\alpha = 1$, $\beta = 1$, $\delta = 1$, $t = 10$, $B = 2$, $\nu = 1$, and $\kappa = 5$.

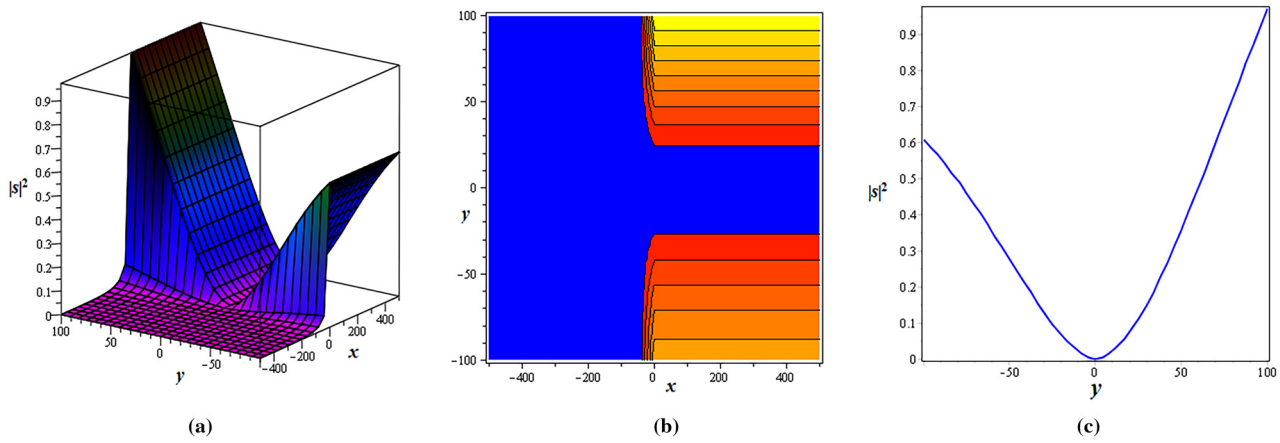

Figure 14: These 3D, contour, and 2D (when $x = 0$) visuals for squared norm $|s|^2$ of the soliton solutions $s_{3,5}(x, y, t)$ in (50) are sketched when $p = 1$, $q = 5$, $r = 4$, $\varrho_1 = 0.91E^{-1}$, $\varrho_2 = 0.12E^{-1}$, $\sigma_1 = 0$, $\sigma_2 = 0.75E^{-2}$, $\kappa_2 = 1$, $\alpha = 0.5$, $\beta = 0.9$, $\delta = 0.1$, $t = 0$, $B = 1$, $\nu = 2$, $\kappa = 5$, and $b_1 = 1$.

support showing a well defined and finite boundary. The emergence of such solitons in the context of CHFSCE suggest integrability in certain limits (due to the availability of peakons), dispersive effect (due to the presence of compacton parabolic soliton), scaling and fractal properties (due to compacton and parabolic interactions) and many more. For instance, these soliton structures may also represent spin wave dynamics such as compacton shows bounded spin wave states, parabolic soliton shows dispersion in spin wave while hump and peakons represent localized spin waves.

Moreover, Figure 11 corresponds to squared norm $|s|^2$ of $s_{1,5}(x, y, t)$ presented in (25), which forms fractal soliton due to the periodic-dark hump soliton profile. Figure 12 corresponds to squared norm $|s|^2$ of $s_{2,1}(x, y, t)$ presented in (32), which forms fractal soliton due to the compacton parabolic soliton profile. Figure 13 corresponds to squared norm $|s|^2$ of $s_{2,10}(x, y, t)$ presented in (41), which forms double peakons soliton profile. Figure 14 corresponds to squared norm $|s|^2$ of $s_{3,5}(x, y, t)$ presented in (50), which forms fractal soliton profile due to the interaction of parabolic soliton with kink soliton. Figure 15 corresponds to squared norm $|s|^2$ of $s_{5,8}(x, y, t)$ presented in (80), which forms peakon soliton profile.

5 Phase portraits and chaotic analysis of the governing system

This section provides phase portraits using bifurcation analysis and time-series analysis to demonstrate the chaotic analysis of the dynamical system.

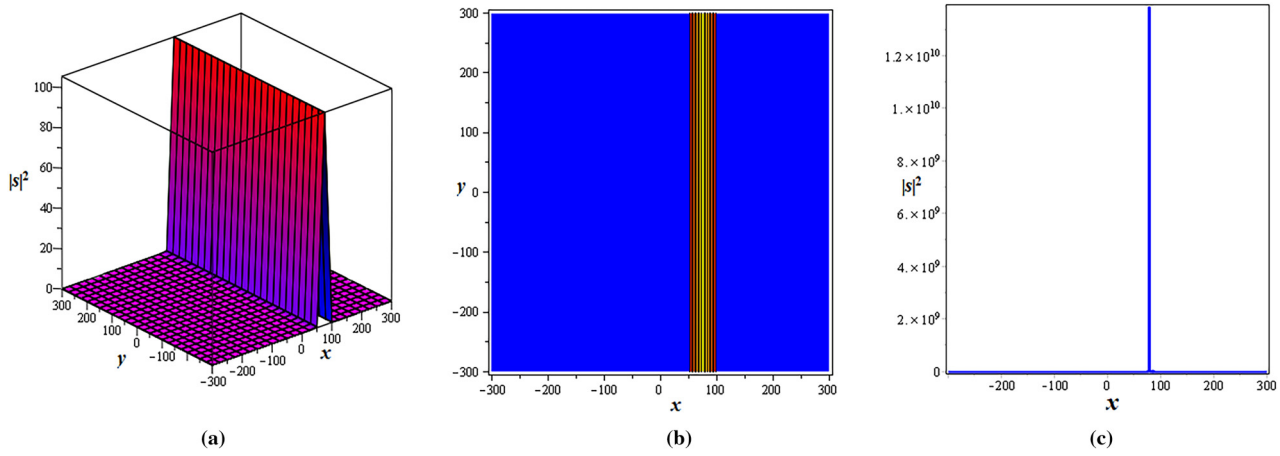

Figure 15: These 3D, contour, and 2D (when $y = 0$) visuals for squared norm $|s|^2$ of the soliton solutions $s_{5,8}(x, y, t)$ in (80) are sketched when $p = 8$, $q = 10$, $r = 2$, $\varrho_1 = 0.22E^{-1}$, $\varrho_2 = 0.15E^{-1}$, $\sigma_1 = 0.25E^{-1}$, $\sigma_2 = 0$, $\kappa_1 = 5$, $\kappa_2 = 1$, $\alpha = 1$, $\beta = 1$, $\delta = 0.3$, $t = 20$, $B = 0$, $\nu = 3$, $\kappa = 1$, $b_0 = 2$, $b_1 = 1$, and $a_0 = 5$.

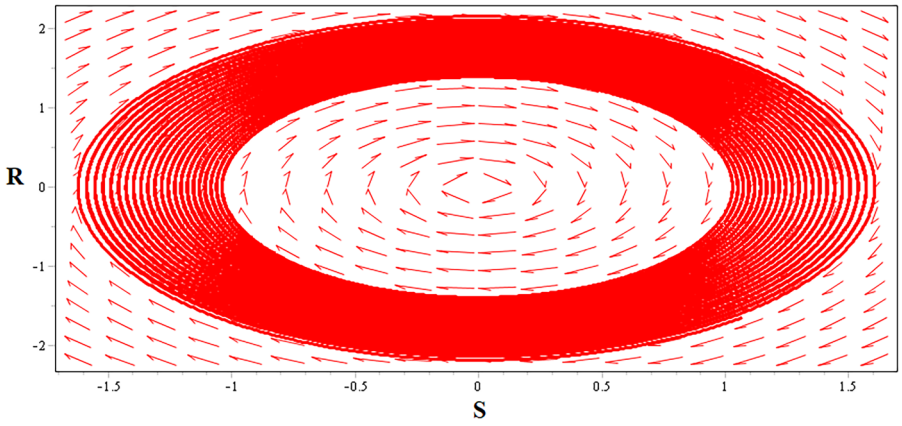

Figure 16: Phase portrait of (88) for $\rho_1 = 0.1$, $\rho_2 = 0.2$, $\omega = 0.2$, $\varrho_1 = 0.3$, $\varrho_2 = 0.2$, $\sigma_1 = 0.5$, $\sigma_2 = 0.1$, $\rho_1 = 0.3$, $\rho_2 = 0.1$, $\rho_3 = 0.2$, and $\rho_4 = 0.003$.

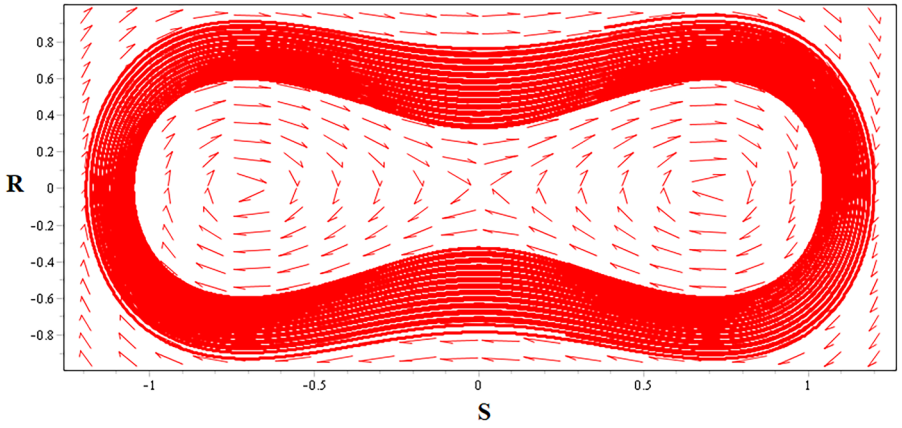

Figure 17: Phase portrait of (88) for $\omega = -3$, $\varrho_1 = 0$, $\varrho_2 = 0$, $\sigma_1 = 1$, $\sigma_2 = 1$, $\rho_1 = 1$, $\rho_2 = 1$, $\rho_3 = 1$, and $\rho_4 = -6$.

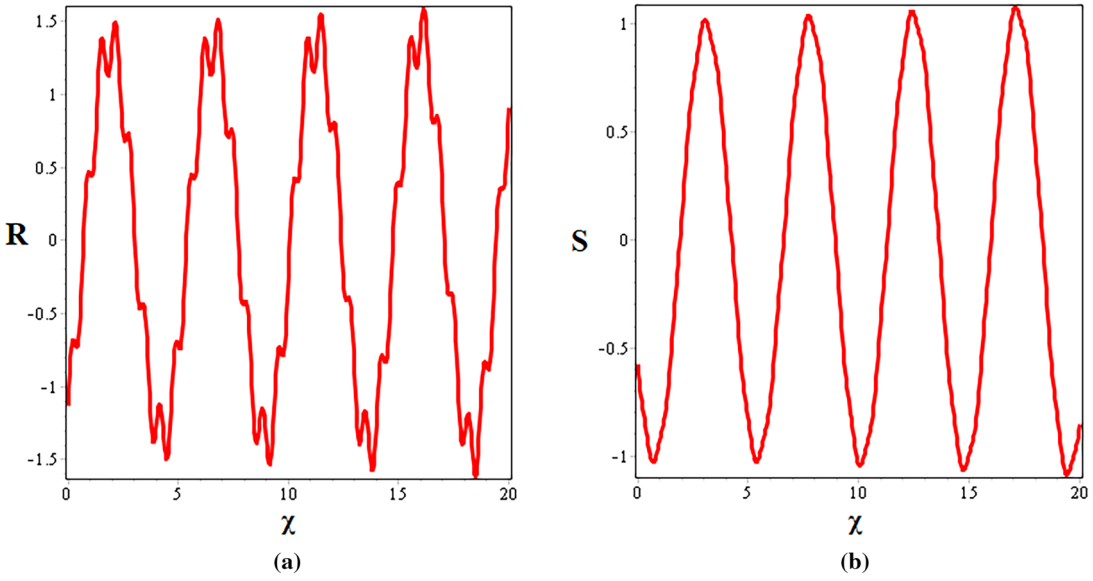

Figure 18: The quasi-periodic pattern in perturbed system (94) for $\rho_1 = 0.1$, $\rho_2 = 0.2$, $\omega = 0.2$, $\varrho_1 = 0.3$, $\varrho_2 = 0.2$, $\sigma_1 = 0.5$, $\sigma_2 = 0.1$, $\rho_1 = 0.3$, $\rho_2 = 0.1$, $\rho_3 = 0.2$, $\rho_4 = 0.003$, $c_0 = 2$, and $\varpi = 3\pi$.

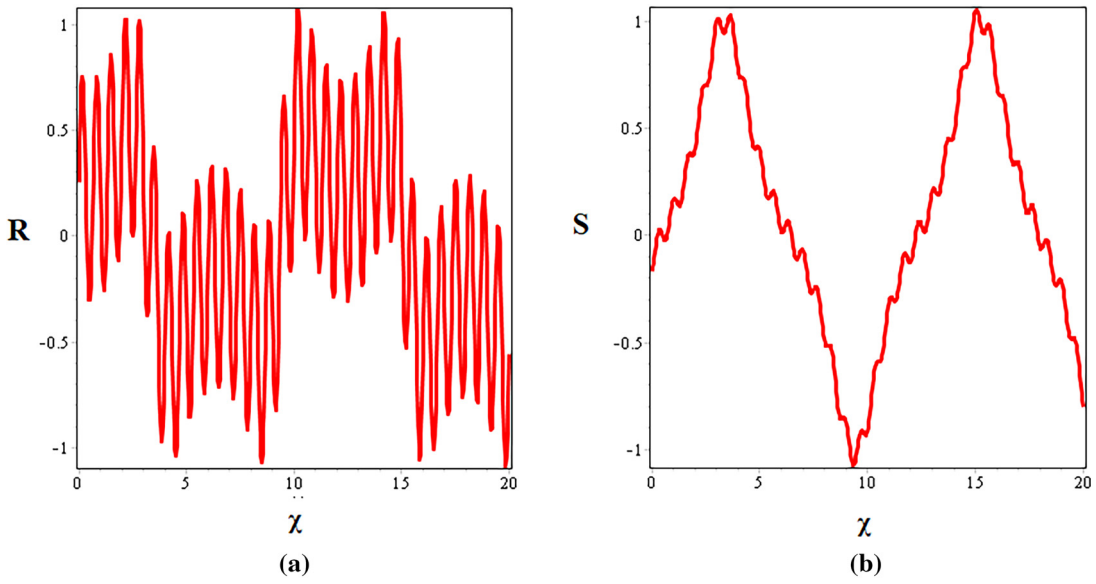

Figure 19: The fractal-like periodic pattern in perturbed system (94) for $\omega = -3$, $\varrho_1 = 0$, $\varrho_2 = 0$, $\sigma_1 = 1$, $\sigma_2 = 1$, $\rho_1 = 1$, $\rho_2 = 1$, $\rho_3 = 1$, $\rho_4 = -6$, $c_0 = 5$, and $\varpi = 3\pi$.

5.1 Bifurcation analysis

Using the concepts of bifurcation theory, we investigate the emergent dynamical system of the CHFSCE. Eq (14)'s planar dynamical system is illustrated as follows:

$$\begin{aligned} g(S,R) &= S' = R, \\ h(S,R) &= R' = A_1 S + A_2 S^3, \end{aligned} \tag{88}$$

where

$$\begin{aligned} A_1 &= \frac{\rho_1 \varrho_1{}^2 + \rho_2 \varrho_2{}^2 + \rho_3 \varrho_1 \varrho_2 - \omega}{\rho_1 \sigma_1{}^2 + \rho_2 \sigma_2{}^2 + \rho_3 \sigma_1 \sigma_2}, \\ A_2 &= \frac{\rho_4}{\rho_1 \sigma_1{}^2 + \rho_2 \sigma_2{}^2 + \rho_3 \sigma_1 \sigma_2}. \end{aligned} \tag{89}$$

This system has a certain integral and demonstrates the ensuing Hamiltonian

$$H(S,R) = \frac{R^2}{2} - \frac{A_1 S^2}{2} - \frac{A_2 S^4}{4}. \tag{90}$$

We examine the bifurcations of phase portraits within the parameterized space denoted by A_1 and A_2 for (88) when the Hamiltonian constant is present. Three equilibrium points are identified by the dynamical system analysis along the S-axis: (0,0), (V_1, 0), and (V_2, 0), where V_1 and V_2 are given by:

$$V_1 = \sqrt{-\frac{A_1}{A_2}}, \quad V_2 = -\sqrt{-\frac{A_1}{A_2}}. \tag{91}$$

Furthermore, according to the Jacobian matrix,

$$J = \begin{bmatrix} \frac{\partial g}{\partial S} & \frac{\partial g}{\partial R} \\ \frac{\partial h}{\partial S} & \frac{\partial h}{\partial R} \end{bmatrix}, \tag{92}$$

The system's Jacobian is

$$|J(S,R)| = -A_1 - 3A_2 S^2. \tag{93}$$

The point is saddle if $|J(S,R)|$ is less than zero, center if it is greater than zero, and cuspidal if it is equal to zero. By adjusting the parameter's values, various results may be obtained.

Remark 1. The closed-circular loop centered at the equilibrium point (0,0) in Figure 16's phase portrait of (88) for $A_1 < 0$ and $A_2 > 0$ suggests that the system is behaving quasi-periodically. This might be seen as an ordered, dynamic evolution brought about by the interaction of many solitonic modes and energy exchange.

Remark 2. In a similar vein Figure 17's phase portrait of (88) for $A_1 > 0$ and $A_2 < 0$ reveals a homoclinic orbit with two centers, suggesting the existence of quasi-periodic soliton in the model.

5.2 Chaotic analysis of the governing system

We use (14) to investigate the chaotic dynamics in the governing system throughout this inquiry. We apply a

perturbation term to the planar dynamical system formed by converting (14) using the Galilean transformation in order to disturb the periodic motion of the system and obtain valuable results of chaotic behavior. Therefore, the following is an expression for the dynamical system of (14) that is perturbed and subject to an external periodic force:

$$\begin{aligned} g(S,R) &= S' = R, \\ f(S,R) &= R' = A_1 S + A_2 S^3 + c_0 \cos(\varpi \chi). \end{aligned} \tag{94}$$

The degree and frequency of the applied external force are represented by the parameters c_0 and ϖ in system (94), respectively. To understand this phenomena, a number of techniques from the corpus of current research are employed, including the Lyapunov exponent, time series, Poincaré map, and phase portrait approaches, to show that the model underlying the perturbed dynamical system exhibits chaotic behavior. The presence of chaotic dynamics in the perturbed nonlinear system is shown in Figures 18 and 19 with initial conditions ($S(\pi) = 1, P(\pi) = -1/\pi$) and with additional suitable parameter values.

Remark 3. The complicated temporal and spatial development of the obtained quasi-periodic solitons is likely the cause of the fractal-like and quasi-periodic oscillations in Figure 18 for $A_1 < 0$ and $A_2 > 0$. Given that quasi-periodic solitons exhibit oscillating behavior in both space and time, the curve's periodicity might be a reflection of this underlying structure. Hence, (94)'s system is quasi-periodic.

Remark 4. Similarly, quasi-periodic solitons are reflected in the fractal-like periodic oscillations for $A_1 < 0$ and $A_2 > 0$ in Figure 19. As a result, the system in (94) is quasi-periodic.

6 Conclusion

In summary, soliton dynamics in complex-structured (3+1)-dimensional CHFSCE involving CFDs was effectively examined and studied in this work. Using the RMESEM, we discovered a range of soliton solutions subjected to the obtained constraint conditions from the model. By the means of 2D, contour, and 3D visual representations, our findings revealed the existence of quasi-periodic solitons such as smooth-, multiple-, and periodic-periodic solitons in the context of CHFSCE, which lead to the formation of fractal structures, whereas the squared norms of the obtained periodic solitons lead to the development of hump, peakon, and parabolic solitons. Additionally, we clarify that in the cases where ($b_1 = 0$) or ($a_0 = 0$) spontaneously occur, the solutions may correspond to solution structures that can be obtained using other techniques such as EDAM, the (G'/G)-expansion method, *etc*. However, in the cases where $b_1 \neq 0$ and $a_0 \neq 0$ spontaneously occur, new wave structures that have not been reported in previous studies are produced. We also study bifurcating and chaotic behavior, observing its presence in the perturbed dynamical system and obtaining favorable outcomes that imply fractal and quasi-periodic motion. The findings we obtained indicated the efficacy of the proposed strategy as a potent approach for discovering new soliton phenomena in the context of such nonlinear settings. Moreover, our findings also showed that the proposed method works well as a strong ansatz method to investigate novel soliton solutions in nonlinear evolution systems. Although the RMESEM has greatly advanced our knowledge of soliton dynamics and how they relate to the models we are studying, it is crucial to recognize the limits of this approach, especially in situations where the nonlinear component and greatest derivative term are not homogenously balanced. Despite this drawback, the current study shows that the approach used in this work is very productive, dependable, and adaptable for nonlinear issues in a range of natural scientific fields. Future goals of this research include figuring out the scaling factors of fractal theory, including fractional derivatives and their effect on fractal solitons, sensitivity of fractal solitons, and stability of the soliton.

Acknowledgments: Ongoing Research Funding Program, (ORF-2025 1060), King Saud University, Riyadh, Saudi Arabia.

Funding information: This project was funded by King Saud University, Riyadh, Saudi Arabia.

Author contributions: Rashid Ali: Conceptualization; Methodology; Writing-original draft; Rabia Imtiaz: Formal analysis; Literature review; Writing-review and editing; Moin-ud-Din Junjua: Supervision; Project administration; Writing-review and editing; Fuad A. Awwad: Data curation; Validation; Visualization; Emad A. A. Ismail: Investigation; Resources; Manuscript revision; Ahmed S. Hendy: Software; Visualization; Writing-review and editing. All authors have accepted responsibility for the entire content of this manuscript and approved its submission.

Conflict of interest: The authors state no conflict of interest.

Data availability statement: The datasets generated and/or analysed during the current study are available from the corresponding author on reasonable request.

References

[1] Shah R, Khan H, Arif M, Kumam P. Application of Laplace-Adomian decomposition method for the analytical solution of third-order dispersive fractional partial differential equations. Entropy. 2019;21(4):335.

[2] Rezazadeh H, Kumar D, Neirameh A, Eslami M, Mirzazadeh M. Applications of three methods for obtaining optical soliton solutions for the Lakshmanan-Porsezian-Daniel model with Kerr law nonlinearity. Pramana. 2020;94:1–11.

[3] Areshi M, Khan A, Shah R, Nonlaopon K. Analytical investigation of fractional-order Newell-Whitehead-Segel equations via a novel transform. Aims Math. 2022;7(4):6936–58.

[4] Iqbal N, Mohammed WW, Alqudah M, Hamza AE, Hussain S. Periodic and axial perturbations of Chaotic solitons in the Realm of complex structured quintic Swift-Hohenberg equation. Math Comput Appl. 2024;29(5):86.

[5] Arshed S. Soliton solutions of fractional complex Ginzburg-Landau equation with Kerr law and non-Kerr law media. Optik. 2018;160:322–32.

[6] Inc M, Yusuf A, Aliyu AI, Baleanu D. Soliton solutions and stability analysis for some conformable nonlinear partial differential equations in mathematical physics. Opt Quantum Electron. 2018;50:1–14.

[7] Zhu C, Al-Dossari M, Rezapour S, Alsallami SAM, Gunay B. Bifurcations, chaotic behavior, and optical solutions for the complex Ginzburg-Landau equation. Results Phys. 2024;59:107601.

[8] Zhu C, Al-Dossari M, Rezapour S, Shateyi S, Gunay B. Analytical optical solutions to the nonlinear Zakharov system via logarithmic transformation. Results Phys. 2024;56:107298.

[9] Zhu C, Abdallah SAO, Rezapour S, Shateyi S. On new diverse variety analytical optical soliton solutions to the perturbed nonlinear Schrodinger equation. Results Phys. 2023;54:107046.

[10] Hussain S, Haq F, Shah A, Abduvalieva D, Shokri A. Comparison of approximate analytical and numerical solutions of the Allen Cahn equation. International J Differ Equ. 2024;2024(1):8835138.

[11] Hussain S, Shah A, Ullah A, Haq F. The q-homotopy analysis method for a solution of the Cahn-Hilliard equation in the presence of advection and reaction terms. J Taibah Univ Sci. 2022;16(1):813–9.

[12] Rahman MU, Khan MI, Haq F, Hayat T. Mathematical modeling and theoretical analysis of second-grade nanomaterial with entropy optimization. Iranian J Sci Tech Trans A Sci. 2019;43:2713–23.

[13] Haq F, Ghazwani HA, Younis J, Ghazwani MH, Alnujaie A. Numerical investigation of mass and heat transfer in ternary hybrid nanofluid flow with activation energy. Int J Energy Res. 2025;2025(1):8061691.

[14] Hussain S, Shah A. Solution of generalized drinfeld-sokolov equations by homotopy perturbation and variational iteration methods. Math Reports. 2013;15(1):49–58.

[15] Pan Z, Pan J, Sang L, Ding Z, Liu M, Fu L, et al. Highly efficient solution-processable four-coordinate boron compound: A thermally activated delayed fluorescence emitter with short-lived phosphorescence for OLEDs with small efficiency roll-off, Chem Eng J. 2024;483:149221.

[16] Liu L, Zhang S, Zhang L, Pan G, Yu J. Multi-UUV Maneuvering counter-game for dynamic target scenario based on fractional-order recurrent neural network. IEEE Trans Cyber. 2023;53:4015–28.

[17] Kai Y, Ji J, Yin Z. Study of the generalization of regularized long-wave equation. Nonlinear Dyn. 2022;107:2745–52.

[18] Ahmad J, Akram S, Noor K, Nadeem M, Bucur A, Alsayaad Y. Soliton solutions of fractional extended nonlinear Schrödinger equation arising in plasma physics and nonlinear optical fiber. Scientif Reports. 2023;13(1):10877.

[19] Ahmad J, Rani S, Turki NB, Shah NA. Novel resonant multi-soliton solutions of time fractional coupled nonlinear Schrödinger equation in optical fiber via an analytical method. Results Phys 2023;52:106761.

[20] Zafar A, Inc M, Shakoor F, Ishaq M. Investigation for soliton solutions with some coupled equations. Opt Quantum Electron. 2022;54(4):243.

[21] Onder I, Secer A, Ozisik M, Bayram M. Investigation of optical soliton solutions for the perturbed Gerdjikov-Ivanov equation with full-nonlinearity. Heliyon. 2023;9(2).

[22] Alsharidi AK, Bekir A. Discovery of new exact wave solutions to the M-fractional complex three coupled Maccari's system by Sardar sub-equation scheme. Symmetry. 2023;15(8):1567.

[23] Manafian J, Foroutan M. Application of $\tan(\phi(\xi)/2)\tan(\phi(\xi)/2)$-expansion method for the time-fractional Kuramoto-Sivashinsky equation. Opt Quantum Electron. 2017;49:1–18.

[24] Gaber A, Ahmad H. Solitary wave solutions for space-time fractional coupled integrable dispersionless system via generalized Kudryashov method. Facta Univ Ser Math Inform. 2021;35:1439–49.

[25] Bibi S, Mohyud-Din ST, Khan U, Ahmed N. Khater method for nonlinear Sharma Tasso-Olever (STO) equation of fractional order. Results Phys. 2017;7:4440–50.

[26] Zheng B, Wen C. Exact solutions for fractional partial differential equations by a new fractional sub-equation method. Adv Differ Equ. 2013;2013:1–12.

[27] Yasmin H, Aljahdaly NH, Saeed AM, Shah R. Investigating symmetric soliton solutions for the fractional coupled Konno-Onno system using improved versions of a novel analytical technique. Mathematics. 2023;11(12):2686.

[28] Yasmin H, Aljahdaly NH, Saeed AM, Shah R. Investigating families of soliton solutions for the complex structured coupled fractional Biswas-Arshed model in birefringent fibers using a novel analytical technique. Fractal Fract. 2023;7(7):491.

[29] Khan H, Shah R, Gómez-Aguilar JF, Baleanu D, Kumam P. Travelling waves solution for fractional-order biological population model. Math Model Natural Phenomena. 2021;16:32.

[30] Zheng B. Exp-function method for solving fractional partial differential equations. Scientif World J. 2013;2013(1):465723.

[31] Ali R, Alam MM, Barak S. Exploring chaotic behavior of optical solitons in complex structured conformable perturbed Radhakrishnan-Kundu-Lakshmanan Model. Phys Scr. 2024;99(9):095209.

[32] Iqbal M, Faridi WA, Ali R, Seadawy AR, Rajhi AA, Anqi AE, et al. Dynamical study of optical soliton structure to the nonlinear Landau-Ginzburg-Higgs equation through computational simulation. Opt Quant Electron 2024;56:1192.

[33] Ali R, Zhang Z, Ahmad H, Alam MM. The analytical study of soliton dynamics in fractional coupled Higgs system using the generalized Khater method. Opt Quantum Electron. 2024;56(6):1067.

[34] Xiao Y, Barak S, Hleili M, Shah K. Exploring the dynamical behaviour of optical solitons in integrable Kairat-II and Kairat-X equations. Phys Scr. 2024;99(9):095261.

[35] Ullah I, Shah K, Barak S, Abdeljawad T. Pioneering the Plethora of soliton for the (3+1)-dimensional fractional Heisenberg ferromagnetic spin chain equation. Phys Scr. 2024;99(9):095229.
[36] Ali R, Barak S, Altalbe A. Analytical study of soliton dynamics in the realm of fractional extended shallow water wave equations. Phys Scr. 2024;99(6):065235.
[37] Ullah I, Shah K, Abdeljawad T, Alam MM, Hendy AS, Barak S. Dynamics behaviours of Kink solitons in conformable Kolmogorov-Petrovskii-Piskunov equation. Qualitative Theory Dyn Syst. 2024;23(Suppl 1):268.
[38] Kudryashov NA. Seven common errors in finding exact solutions of nonlinear differential equations. Commun Nonl Sci Numer Simulat. 2009;14(9-10):3507–29.
[39] Navickas Z, Ragulskis M. Comments on “A new algorithm for automatic computation of solitary wave solutions to nonlinear partial differential equations based on the Exp-function method”. Appl Math Comput. 2014;243:419–25.
[40] Antonova AO, Kudryashov NA. Generalization of the simplest equation method for nonlinear non-autonomous differential equations. Commun Nonlinear Sci Numer Simulat. 2014;19(11):4037–41.
[41] Navickas Z, Marcinkevicius R, Telksniene I, Telksnys T, Ragulskis M. Structural stability of the hepatitis C model with the proliferation of infected and uninfected hepatocytes. Math Comput Model Dyn Syst. 2024;30(1):51–72.
[42] Martin-Vergara F, Rus F, Villatoro FR. Fractal structure of the soliton scattering for the graphene superlattice equation. Chaos Solitons Fractals. 2021;151:111281.
[43] Wang K. A new fractal model for the soliton motion in a microgravity space. Int J Numer Methods Heat Fluid Flow. 2021;31(1):442–51.
[44] Zheng CL. Coherent soliton structures with chaotic and fractal behaviors in a generalized (2+1)-dimensional Korteweg de-Vries system. Chinese J Phys. 2003;41(5):442–55.
[45] Bunde A, Havlin S (Eds.). Fractals in science. Heidelberg: Springer; 2013.
[46] Stanley HE. Fractal landscapes in physics and biology. Phys A Stat Mech Appl. 1992;186(1–2):1–32.
[47] Bizzarri M, Giuliani A, Cucina A, D’Anselmi F, Soto AM, Sonnenschein C. Fractal analysis in a systems biology approach to cancer. In Seminars Cancer Biology. Vol. 21, No. 3. Academic Press. 2011, June, p. 175–82.
[48] Latha MM, Vasanthi CC. An integrable model of (2+1)-dimensional Heisenberg ferromagnetic spin chain and soliton excitations. Phys Scr. 2014;89(6):065204.
[49] Ma YL, Li BQ, Fu YY. A series of the solutions for the Heisenberg ferromagnetic spin chain equation. Math Meth Appl Sci. 2018;41(9):3316–22.
[50] Devnath S, Khatun MM, Akbar MA. Analytical solutions and soliton behaviors in the space fractional Heisenberg ferromagnetic spin chain equation. Partial Differ Equ Appl Math. 2024;11:100783.
[51] Hashemi MS. Some new exact solutions of (2+1)-dimensional nonlinear Heisenberg ferromagnetic spin chain with the conformable time fractional derivative. Opt Quantum Electron. 2018;50(2):79.
[52] Ur Rahman M, Sun M, Boulaaras S, Baleanu D. Bifurcations, chaotic behavior, sensitivity analysis, and various soliton solutions for the extended nonlinear Schrödinger equation. Boundary Value Problems. 2024;2024(1):15.
[53] Chahlaoui Y, Ali A, Ahmad J, Javed S. Dynamical behavior of chaos, bifurcation analysis and soliton solutions to a Konno-Oono model. PLoS One. 2023;18(9):e0291197.
[54] Sene N. Analysis of a fractional-order chaotic system in the context of the Caputo fractional derivative via bifurcation and Lyapunov exponents. J King Saud Univ-Sci. 2021;33(1):101275.
[55] Iqbal SA, Hafez MG, Uddin MF. Bifurcation features, chaos, and coherent structures for one-dimensional nonlinear electrical transmission line. Comput Appl Math. 2022;41(1):50.
[56] Javed S, Ali A, Ahmad J, Hussain R. Study the dynamic behavior of bifurcation, chaos, time series analysis and soliton solutions to a Hirota model. Opt Quantum Electron. 2023;55(12):1114.
[57] Jamal T, Jhangeer A, Hussain MZ. Analysis of nonlinear dynamics of Novikov-Veselov equation using solitonic solutions, bifurcation, periodic and quasi-periodic solutions, and poincaré section. European Phys J Plus. 2023;138(12):1087.
[58] Okereke RN, Maliki SO. Asymptotic behaviour of solutions of certain third order nonlinear differential equations via phase portrait analysis. Appl Math. 2016;7(18):2324–35.
[59] Muflih Alqahtani A, Akram S, Alosaimi M. Study of bifurcations, chaotic structures with sensitivity analysis and novel soliton solutions of non-linear dynamical model. J Taibah Univ Sci. 2024;18(1):2399870.
[60] Hosseini K, Hinçal E, Ilie M. Bifurcation analysis, chaotic behaviors, sensitivity analysis, and soliton solutions of a generalized Schrödinger equation. Nonl Dyn. 2023;111(18):17455–62.
[61] Tarasov VE. On chain rule for fractional derivatives. Commun Nonl Sci Numer Simulat. 2016;30(1–3):1–4.
[62] He JH, Elagan SK, Li ZB. Geometrical explanation of the fractional complex transform and derivative chain rule for fractional calculus. Phys Lett A. 2012;376(4):257–9.
[63] Sarikaya MZ, Budak H, Usta H. On generalized the conformable fractional calculus. TWMS J Appl Eng Math. 2019;9(4):792–9.
[64] Bilal M, Iqbal J, Ali R, Awwad FA, Ismail EAA. Establishing breather and N-soliton solutions for conformable Klein-Gordon equation. Open Phys. 2024;22(1):20240044.
[65] Ali R, Kumar D, Akgul A, Altalbe A. On the periodic soliton solutions for fractional schrödinger equations. Fractals, World Scientific Publisher; 2024.
[66] Fan E. Extended tanh-function method and its applications to nonlinear equations. Phys Lett A. 2000;277(4–5):212–8.
[67] Zhang JL, Wang ML, Wang YM, Fang ZD. The improved F-expansion method and its applications. Phys Lett A. 2006;350(1–2):103–9.

Appendix

Several analytical techniques rely on the Riccati equation as their foundation. These methods are helpful for analyzing soliton occurrences in nonlinear models since the Riccati equation exhibits solitary solutions [41]. These applications of the Riccati hypothesis served as inspiration for the current study, which created and applied the Riccati equation-incorporating RMESEM to generate and assess soliton dynamics in CHFSCE [34]. The adjustment was advantageous since it produced a large number of additional soliton solutions for the selected model in the rational, exponential, hyperbolic, periodic, and rational-hyperbolic families of solutions. The given solutions significantly advance our understanding of soliton dynamics by enabling us to relate the observations in the focused model to underlying theories. Limiting our technique's solutions results in specific solutions from other approaches. The analogy is given in subsection:

A.1 Comparison with alternative analytical techniques

Our method produces results that are exactly the same as those of a number of different analytical methods. For instance,

Axiom 7.1.1: The subsequent solution structure is formed by setting $b_1 = 0$ in (15)

$$S(\mathfrak{Z}) = b_0 + a_0\left(\frac{1}{U(\mathfrak{Z})}\right). \tag{A1}$$

This displays the closed form solution for EDAM and the F-expansion approach. Thus, our results can also lead to the solutions obtained by EDAM [64,65] and the F-expansion technique, attaining $b_1 = 0$.

Axiom 7.1.2: Similarly, after substituting $a_0 = 0$ in Eq. (15), the following structure of the solution is formed:

$$S(\mathfrak{Z}) = \sum_{j=0}^{1} b_j\left(\frac{U'(\mathfrak{Z})}{U(\mathfrak{Z})}\right)^j. \tag{A2}$$

This is the closed form solution that is obtained by incorporating the Riccati equation with (G'/G)-expansion approach.

Consequently, the results of our investigation may provide a wider range of solutions generated by the (G'/G)-expansion technique [29], the tan-function method [66], F-expansion method [67], and EDAM [28].